UNIVERSIDADE DA BEIRA INTERIOR
Ciências da Saúde

Desenvolvimento e funcionalização de nanopartículas de ouro com revestimento de sílica para aplicação na terapia do cancro

Ana Carolina Félix Rodrigues

Dissertação para obtenção do Grau de Mestre em
Ciências Biomédicas
(2º ciclo de estudos)

Orientador: Prof. Doutor Ilídio Joaquim Sobreira Correia
Co-orientador: Mestre André Ferreira Moreira

Covilhã, junho de 2018

Aos meus pais, por tornarem tudo possível…

“If you can’t fly, then run.
If you can’t run, then walk.
If you can’t walk, then crawl,
but whatever you do,
you have to keep moving forward.”

Martin Luther King Jr

Agradecimentos

Em primeiro lugar gostaria de agradecer ao meu orientador Professor Ilídio Correia, pela oportunidade de integrar e trabalhar no seu grupo de investigação. A sua exigência, orientação e recomendações contribuíram para o desenvolvimento desta tese, e foram cruciais para o meu crescimento pessoal e profissional.

Ao meu co-orientador, André Moreira, sou profundamente grata por toda ajuda, paciência e por todo o tempo que despendeu comigo ao longo desta tese. Agradeço pela constante troca de ideias, por todo o conhecimento que me transmitiu e pela sua boa disposição, mesmo nos momentos de maior stress. Sem o seu apoio e orientação este trabalho não teria sido possível.

Aos meus colegas do grupo de investigação, gostaria de agradecer pelo seu apoio, incentivo, por estarem sempre prontos ajudar, e por todos os bons momentos que proporcionaram. À Catarina, a minha parceira de trabalho, agradeço por toda ajuda, pela sua energia e alegria contagiante. À Sol um muito obrigada pelas boleias, sorrisos, brincadeiras e por descobrir que somos mais parecidas do que imaginávamos… À Cátia e Sofia, um obrigado por embarcarem comigo nesta aventura. Por fim, um agradecimento muito especial ao André, Beta, Duarte, e Sónia, por provarem que a exigência e trabalho não são ausência de boa disposição.

Às minhas meninas, Andreia, Cátia, Chica, Inês e Rita, obrigado por mais do que amigas serem as minhas irmãs do coração. Obrigada por me aturarem, pela paciência, pelo incentivo e força. Obrigada por estes 5 anos. Obrigado por este ano e por todos os dias, que são sempre especiais e uma verdadeira aventura na vossa companhia. Obrigada pelos sorrisos e por todos os bons momentos, mas acima de tudo obrigada pela vossa amizade… “Os bons amigos conhecem todas as nossas histórias. Os melhores amigos fazem parte delas.”

Por fim, agradeço àqueles que proporcionaram tudo isto. Aos meus pais, Amália e Francisco, cujos agradecimentos são poucos, e a quem sou eternamente grata por toda a paciência, sacrifícios, apoio e amor incondicional. À minha mãe que me conhece melhor que ninguém, obrigada pelos conselhos prudentes, infinito encorajamento e confiança em mim. Ao meu pai, agradeço pela sua paciência, confiança e pelas poucas palavras que tantas vezes dizem tanto.

Resumo

O cancro é uma das principais causas de morte em todo o mundo, e durante os últimos anos a sua incidência tem vindo a aumentar. Além disso, os tratamentos atualmente disponíveis na clínica, como a cirurgia, radioterapia e quimioterapia, caracterizam-se por apresentarem uma baixa eficácia terapêutica e toxicidade inespecífica. Em particular, os agentes utilizados em quimioterapia são pouco solúveis, rapidamente degradados ou removidos da corrente sanguínea e ainda, apresentam uma baixa seletividade para as células cancerígenas. Devido a estas limitações, existe uma crescente procura por novas terapias anticancerígenas. Entre as diversas abordagens desenvolvidas, os recentes avanços na área da nanotecnologia abriram o caminho para uma nova era de terapias contra o cancro. As nanopartículas podem ser produzidas com diferentes materiais e geometrias. Entre estas, as nanopartículas de ouro revestidas com sílica mesoporosa (Au-MSS) apresentam propriedades físico-químicas e biológicas, que as tornam numa das nanoplataformas mais promissoras para a terapia do cancro. No entanto, a aplicação bem-sucedida das Au-MSS na clínica é dificultada pela libertação descontrolada dos agentes terapêuticos, pelo seu reduzido tempo de meia vida na circulação sanguínea e pelas propriedades farmacocinéticas desfavoráveis.

O plano de trabalho desenvolvido nesta dissertação teve como objetivo projetar e produzir Au-MSS funcionalizadas na sua superfície com polímeros biofuncionais, de forma a permitir o controlo da libertação dos agentes terapêuticos, aumentar o tempo de circulação na corrente sanguínea e, fundamentalmente, potenciar o seu efeito terapêutico. Para este propósito, duas metodologias, interação eletrostática e ligação química, foram otimizadas para funcionalizar as Au-MSS em forma de bastonete com succinato de D-α-tocoferil polietilenoglicol 1000 (TPGS) e polietilenoimina ramificada (PEI). O TPGS foi selecionado tendo por base a sua natureza anfifílica, de forma a aumentar a solubilidade e, consequentemente, a estabilidade coloidal das nanopartículas. Por outro lado, o PEI devido à sua natureza catiónica será atraído para a superfície da sílica mesoporosa, que possui carga negativa, bloqueando os poros das partículas e, consequentemente, a libertação do fármaco neles encapsulado. Além disso, devido à sua forma de bastonete, as Au-MSS permitem combinar a entrega direcionada de fármacos com a terapia fototérmica.

As Au-MSS produzidas no âmbito desta tese exibiam uma morfologia uniforme com um núcleo de ouro e um revestimento de sílica bem definidos. A carga superficial das nanopartículas mostrou-se dependente do processo de síntese. As partículas modificadas por interações eletrostáticas (Au-MSS/TPGS-PEI) apresentaram valores de potencial zeta negativos (-16,9 e -5,1 mV), enquanto que as formulações produzidas por ligação química (Au-MSS/TPGS/PEI) resultaram em nanopartículas carregadas positivamente (+30,9 e +6,8 mV). O sucesso da ligação dos polímeros às nanopartículas foi confirmado por espectroscopia de infravermelho por

transformada de Fourier e análise termogravimétrica. A funcionalização das Au-MSS mostrou não afetar a capacidade fototérmica das nanopartículas, no entanto as Au-MSS/TPGS/PEI apresentaram uma menor eficiência de encapsulamento do fármaco. Nos ensaios *in vitro* foi demonstrada a biocompatibilidade das Au-MSS e Au-MSS/TPGS-PEI até concentrações de 200 μg/mL, contudo as formulações carregadas positivamente só revelaram ser biocompatíveis até 100 μg/mL e 125 μg/mL.

Em suma, os resultados apresentados nesta tese confirmam que a modificação das Au-MSS utilizando os polímeros TPGS e PEI foi bem-sucedida. Por outro lado, foi também demonstrado o potencial das Au-MSS para serem aplicadas na terapia anticancerígena, onde podem realizar simultaneamente entrega de fármacos, fototerapia e imagiologia.

Palavras-chave

Cancro, Nanopartículas de Ouro com Revestimento de Sílica, PEI, Terapia Fototérmica, TPGS.

Resumo Alargado

Atualmente o cancro constitui uma das principais causas de morte em todo o mundo, apresentando uma incidência crescente na população mundial. Os tratamentos convencionais como a cirurgia, radioterapia e quimioterapia caracterizam-se por apresentar uma baixa eficácia terapêutica e toxicidade não específica, o que despoleta diferentes efeitos secundários. A quimioterapia é a abordagem terapêutica mais utilizada na clínica. No entanto, esta apresenta diversas desvantagens relacionadas com a falta de especificidade e a rápida degradação dos agentes quimioterápicos, o que leva a que estes apresentem uma baixa biodisponibilidade. A baixa eficácia terapêutica aliada aos efeitos secundários realçam a necessidade de desenvolver novas terapias anticancerígenas.

Os recentes desenvolvimentos na área da Nanotecnologia permitiram o desenvolvimento de novas estratégias, capazes de ultrapassar as desvantagens associadas às terapias atuais, abrindo caminho para uma nova era de medicamentos que possam ser usados no tratamento do cancro. Os sistemas à escala nanométrica (nanopartículas) constituem uma abordagem promissora, uma vez que possuem a capacidade de encapsular fármacos, prevenir a sua degradação prematura, controlar a sua libertação e direcioná-los especificamente para as células cancerígenas. Paralelamente, a terapia fototérmica tem atraído a atenção de diferentes investigadores em todo o mundo. Esta abordagem explora materiais que são capazes de se acumular preferencialmente no tecido tumoral, e que após a sua exposição a estímulos específicos (por exemplo, campo magnético e radiação de infravermelho próximo) induzem um aumento de temperatura, o que leva a efeitos citotóxicos nas células cancerígenas. Desta forma, a terapia combinatória mediada por nanopartículas, é uma das abordagens mais exploradas para melhorar a eficácia das terapias atualmente disponíveis. Entre as diferentes nanopartículas investigadas até ao momento, as nanopartículas de ouro revestidas com sílica mesoporosa (Au-MSS) apresentam propriedades estruturais únicas, que permitem a sua aplicação simultânea na terapia e imagiologia. A atenuação de raios X, o efeito de Raman e a absorção na região do infravermelho próximo, que são características do núcleo de ouro, suportam a aplicação destas nanopartículas como agentes de imagiologia. Para além disto, o ouro também pode ter a capacidade de converter a radiação proveniente de uma fonte de luz em calor, e desta forma exercer efeitos citotóxicos nas células cancerígenas. Este aumento local de temperatura pode sensibilizar as células para a ação dos fármacos (termosensibilização), potenciando o efeito terapêutico destes, ou mesmo promover a morte celular (destabilização da membrana celular ou desnaturação do material genético e proteínas). Por outro lado, a inclusão da camada de sílica mesoporosa protege o núcleo de ouro de fenómenos de degradação e agregação, fornecendo ainda uma capacidade de carga adicional para encapsular as moléculas terapêuticas. No entanto, a aplicação bem-sucedida das Au-MSS como nanoestruturas eficientes

no combate ao cancro é dificultada pela libertação descontrolada dos agentes terapêuticos, o reduzido tempo de meia vida na circulação sanguínea e uma farmacocinética desfavorável.

O plano de trabalho realizado no âmbito desta dissertação teve como objetivo projetar e produzir Au-MSS modificadas na sua superfície com polímeros biofuncionais, de forma a controlar o perfil de libertação dos agentes terapêuticos, aumentar o tempo de circulação da partícula na corrente sanguínea e, fundamentalmente, potenciar o seu efeito terapêutico. Para este propósito, duas metodologias, interação eletrostática e ligação química, foram otimizadas para funcionalizar as Au-MSS em forma de bastonete com succinato de D-α-tocoferil polietilenoglicol 1000 (TPGS) e polietilenoimina ramificada (PEI). O TPGS, um derivado da vitamina E, foi selecionado com base na sua natureza anfifílica de forma a aumentar a solubilidade e a estabilidade coloidal das nanopartículas. Por outro lado, pode também atuar como um inibidor da glicoproteína P (P-gp) e desta forma permitir o aumento da biodisponibilidade dos agentes quimioterápicos. O PEI, devido à sua natureza catiónica será atraído para a superfície da sílica mesoporosa, de carga negativa, bloqueando os poros das partículas e, consequentemente, a libertação do fármaco neles encapsulados. Para além disso, a protonação dos grupos amina, quando em ambiente ácido, também promoverá a fuga das nanopartículas das vesículas endocíticas e dos lisossomas.

As Au-MSS produzidas no âmbito desta dissertação exibem uma morfologia uniforme (forma de bastão), com núcleo de ouro e um revestimento de sílica bem definidos. De forma a funcionalizar as Au-MSS, o TPGS e PEI foram alvo de modificações químicas. Para promover a adsorção electroestática na superfície das Au-MSS, as cadeias do TPGS foram ligadas quimicamente ao PEI utilizando o 1,1-carbonildiimidazol (CDI). Por outro lado, para a ligação química do TPGS e PEI na superfície das Au-MSS, ambos os polímeros foram modificados utilizando isocianato de 3-propil-trietoxisilano (TESPIC). Desta forma, a carga superficial das nanopartículas mostrou-se dependente do processo de síntese. As partículas modificadas por interações eletrostáticas (Au-MSS/TPGS-PEI) apresentaram um potencial zeta com valores negativos (-16,9 e -5,1 mV), enquanto que as formulações produzidas por ligação química (Au-MSS/TPGS/PEI) resultaram em nanopartículas carregadas positivamente (+30,9 e +6,8 mV). O sucesso da ligação dos polímeros às nanopartículas foi confirmado por espectroscopia de infravermelho por transformadas de Fourier e análise termogravimétrica. A funcionalização das Au-MSS mostrou não afetar a capacidade fototérmica das nanopartículas, tendo todas as formulações atingido variações de temperatura de cerca 40 ºC. No entanto, as Au-MSS/TPGS/PEI apresentaram uma menor eficiência de encapsulamento do fármaco. Ensaios *in vitro* demostraram a biocompatibilidade das Au-MSS e Au-MSS/TPGS-PEI até concentrações de 200 µg/mL, contudo as formulações carregadas positivamente só se mantiveram biocompatíveis até 100 µg/mL e 125 µg/mL. Adicionalmente, por microscopia de confocal foi possível confirmar que as diferentes formulações podem ser internalizadas pelas células cancerígenas, e desta forma permitir a entrega de fármacos no interior das células evitando a

sua degradação no meio extracelular, potenciando o efeito terapêutico. Entre as formulações testadas, as Au-MSS/TPGS-PEI apresentaram os resultados físico-químicos e biológicos mais promissores, seguidas pelas Au-MSS/TPGS/PEI (3:1).

Em suma, os resultados apresentados nesta tese confirmam que a modificação da superfície das Au-MSS com polímeros TPGS e PEI foi realizada com sucesso. Adicionalmente, foi também confirmado o potencial das Au-MSS para aplicação na terapia do cancro, onde podem realizar simultaneamente entrega de fármacos, fototerapia e imagiologia.

Abstract

Cancer is one of the leading causes of death in the world and its incidence has been increasing over the years. On the other side, the currently available treatments, such as surgery, radiotherapy, and chemotherapy, are characterized by presenting a low efficacy and non-specific toxicity. Particularly, the chemotherapeutic agents are poorly soluble, rapidly degraded or removed from blood circulation and present low selectivity towards the cancer cells. Therefore, there is a huge demand for novel and more effective anti-cancer therapeutics. The recent breakthroughs in nanotechnology paved the way for a new era of anti-cancer medicines. Nanoparticles can be produced with different materials and organizations, among them, the gold-core silica shell (Au-MSS) nanoparticles present advantageous physicochemical and biological properties that make them a promising nanoplatform for cancer therapy. Nevertheless, the successful application of Au-MSS nanoparticles as an effective cancer nanomedicine is hindered by the uncontrolled release of the therapeutic payloads, limited blood circulation time and unfavorable pharmacokinetics.

This dissertation work plan aimed at designing and developing a novel Au-MSS surface modification with biofunctional polymers for overcoming the uncontrolled drug release profile, limited nanoparticles' blood circulation time and ultimately potentiate the therapeutic effect. For that purpose, two different methodologies, electrostatic interaction or chemical linkage, were explored and optimized to functionalize Au-MSS, displaying a rod-like shape, with D-α tocopherol polyethylene glycol 1000 succinate (TPGS) and branched polyethyleneimine (PEI). TPGS was selected based on its amphiphilic nature that can act as solubilizer and consequently increase the particles' colloidal stability. On the other side, PEI due to its cationic nature will be attracted to the negatively charged mesoporous silica surface blocking the particle' pores and consequently the drug release. Additionally, the rod-like shape of Au-MSS allows the combination of drug delivery with photothermal therapy.

The produced Au-MSS nanorods display a uniform morphology and a well-defined gold nucleus and silica shell. Further, the particles' surface charge was dependent on the synthesis methodology. The particles modified by electrostatic interactions (Au-MSS/TPGS-PEI) were negative (-16.9 and -5.1 mV) whereas the formulations produced by chemical linkage (Au-MSS/TPGS/PEI) resulted in positively charged nanoparticles (+30.9 and +6.8 mV). The successful incorporation of the polymers was confirmed by Fourier Transformed Infrared spectroscopy and thermogravimetric analysis. Moreover, the Au-MSS functionalization did not affect the particles photothermal capacity. However, the Au-MSS/TPGS/PEI nanorods displayed a decreased drug encapsulation efficiency. In vitro assays demonstrated the biocompatibility of Au-MSS and Au-MSS/TPGS-PEI up to concentrations of 200 μg/mL, however, the positively charged formulations only remained biocompatible until 100 and 125 μg/mL.

Overall, the results presented in this thesis confirm the successful modification of Au-MSS nanorods with TPGS and PEI. Additionally, it was also demonstrated the potential of Au-MSS formulations for being applied in cancer therapy, where they can act simultaneously as photothermal, drug delivery and bioimaging agents.

Keywords

Cancer, Gold Core Silica Shell Nanoparticles, PEI, Photothermal Therapy, TPGS.

List of Publications

Articles in peer-reviewed international journals:

Moreira, A. F.*, Rodrigues, C. F.*, Reis, C. A.*, Costa, E. C., and Correia, I. J. (2018). "Gold-core silica shell nanoparticles application in imaging and therapy: A review." Microporous and Mesoporous Materials. 270:168-179. DOI:10.1016/j.micromeso.2018.05.022.

Rodrigues, C. F., Reis, C. A., Moreira, A. F., Ferreira, P., and Correia, I. J. "Optimization of gold core-mesoporous silica shell functionalization with TPGS and PEI for cancer therapy." *Submitted for publication*.

Moreira, A. F., Rodrigues, C. F., Reis, C. A., Costa, E. C., Ferreira, P., and Correia, I. J. "Development of poly(2-ethyl-2-oxazoline) coated gold-core silica shell nanorods for the chemo-photothermal cancer therapy." *Submitted for publication*.

*****These authors contributed equally to this article**.**

Index

Figure Index

List of Abbreviations

AA	L-ascorbic acid
ANOVA	One-way analysis of variance
ATP	Adenosine triphosphate
AR	Aspect ratio
Au-MSS	Gold core and mesoporous silica shell
Au-MSS/TPGS-PEI	Au-MSS modified by electrostatic interactions
Au-MSS/TPGS-PEI (1 min)	Au-MSS/TPGS-PEI vortexed for 1 min
Au-MSS/TPGS-PEI (5 min)	Au-MSS/TPGS-PEI vortexed for 5 min
Au-MSS/TPGS/PEI	Au-MSS produced by chemical linkage
Au-MSS/TPGS/PEI (1:1)	Au-MSS/TPGS/PEI with TPGS/PEI ratio (1:1)
Au-MSS/TPGS/PEI (3:1)	Au-MSS/TPGS/PEI with TPGS/PEI ratio (3:1)
A549	Human lung carcinoma
Bcl-2	B-cell lymphoma 2
CDI	1,1'-Carbonyldiimidazole
CLSM	Confocal laser scanning microscopy
CT	Computerized tomography
CTAB	Cetyltrimethylammonium bromide
DMEM-HG	Dulbecco's modified eagle medium-high glucose
DNA	Deoxyribonucleic acid
Dox	Doxorubicin hydrochloride
ECM	Extracellular matrix
EE	Encapsulation efficiency
EPR	Enhanced permeability and retention
EtOH	Ethanol
FBS	Fetal bovine serum
FITC	Fluorescein 5-isothiocyanate
FTIR	Fourier transform infrared spectroscopy
HeLa	Human negroid cervix epithelioid carcinoma
HepG2	Liver hepatocellular carcinoma
K^-	Negative control
K^+	Positive control
MDR	Multidrug resistance
MRI	Magnetic resonance imaging
NIR	Near infrared
PA	Photoacoustic
PBS	Phosphate-buffered saline
PDT	Photodynamic therapy

PEG	Polyethylene glycol
PEI	Polyethyleneimine
PEOZ	Polyoxazolines
PGA	Polyglycerol acid
P-gp	Glycoprotein-P
PTT	Phothermal therapy
RES	Reticuloendothelial system
RGD	Arginylglycylaspartic acid
RVG29	29 residue peptide derived from rabies virus glycoprotein
SERS	Surface enhanced raman spectroscopy
TEM	Transmission electron microscopy
TEOS	Tetraethyl orthosilicate
TESPIC	3-(Triethoxysilyl)propyl isocyanate
TESPIC-PEI	TESPIC modified PEI
TESPIC-TPGS	TESPIC modified TPGS
TGA	Thermogravimetric analysis
THF	Tetrahydrofuran
TME	Tumor microenvironment
TPGS	D-α tocopherol polyethylene glycol 1000 succinate
TPGS-PEI	TPGS linked to PEI
UK	United Kingdom
USA	United States of America
UV-vis	Ultraviolet-visible
WGA-Alexa Fluor 594®	Wheat germ agglutinin conjugate Alexa 594®

Chapter 1

Introduction

This chapter is based on the publication entitled: “Gold-Core Silica Shell Nanoparticles Application in Imaging and Therapy: a Review” (2018). Microporous and Mesoporous Materials. 270: 168-179.

1. Introduction

1.1. Cancer

1.1.1. Cancer epidemiology

Cancer is a major healthcare problem causing millions of deaths around the globe. Worldwide data from 2012 indicate that occurred more than eight million cancer-related deaths and fourteen million new cases of cancer were diagnosed (1). In the current year, it is estimated that more than one million seven hundred thousand new cases will be diagnosed and that almost six hundred thousand cancer-related deaths will occur only in the United States of America (USA) (2). In Portugal, accordingly to the recent studies from the *Direção Geral de Saúde* (2017), there has been an increase in the cancer incidence at a rate of 3 % per year. Further, it is predicted that in the year of 2035 the cancer incidence and mortality would be close to sixty thousand and thirty thousand cases, respectively (3).

Several risks factors have been associated to these alarming predictions of cancer mortality and incidence, such as the exposure to environmental agents (*e.g.* radiations and pollution), lifestyle (*e.g.* alcohol, diet, tobacco, and drugs), genetical predisposition as well as the global population aging and growth (1, 4). The cancer prevalence is dependent on the population gender and age. For example, the lung, prostate, colorectal, and stomach cancers are the most prevalent in men, while in women, breast, colorectal, lung and cervical are the most common ones (1).

1.1.2. Cancer development and main hallmarks

Cancer is a highly complex disease that is originated by an uncontrolled cellular proliferation – denominated carcinogenesis - where normal cells suffer profound genetic and epigenetic transformations that lead to the development of malignant cells (5). In fact, cancer corresponds to a family of diseases that share several key characteristics and can affect the different organs of the body (6). Initially, cancer was described as a mass of cancer cells that display a continuous and unlimited proliferation, with the potential to invade the surrounding tissues or even extravasate to other sites in the body (7, 8). However, the concept of cancer evolved to a complex and heterogeneous tissue in a dynamic interplay with surrounding stromal cells and non-cellular elements, that constitute the tumor microenvironment (TME) (Figure 1) (9, 10). Apart from cancer cells, the TME is comprised of endothelial cells, pericytes, cancer-associated fibroblasts, immune system cells, extracellular matrix (ECM) components, and signaling molecules.

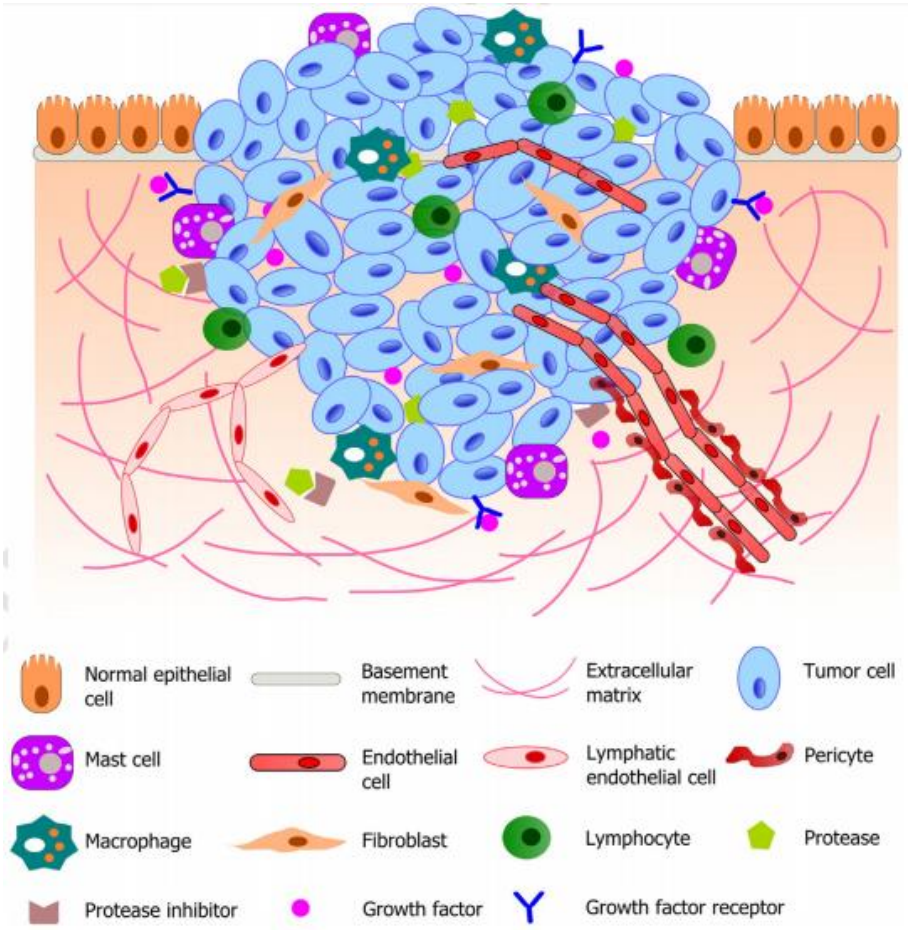

Figure 1 - Representation of the cancer tissue heterogeneity. Complex TME characterized by the cross-talking between malignant, endothelial, pericytes, fibroblasts, immune system cells, and the ECM (adapted from (11)).

The interactions between the different elements of TME play a critical role in the tumor progression since their cross-talking can trigger invasion, pro-survival, and proliferative pathways that are essential for the cancer establishment and development (5, 9, 12). Further, in response to this complex interaction, cancer cells develop or maintain certain key characteristics designated as "hallmarks of cancer" (Figure 2), initially described by Hanahan and Weinberg (7, 13).

One of the most important characteristics of cancer cells is their capacity to maintain the proliferative signaling. In this process, cancer cells acquire the autonomy to produce their own growth signals (*e.g.* platelet-derived growth factor) or overexpress receptors involved in cell growth pathways, becoming less dependent of the surrounding tissue (8, 13). Simultaneously, cancer cells also develop the capacity to evade the programmed cell death, principally by bypassing pro-apoptotic signals (*e.g.* tumor suppressor protein 53 and retinoblastoma protein) or promoting the overexpression of anti-apoptotic proteins, such as those of B-cell lymphoma 2 (Bcl-2) family (14, 15).

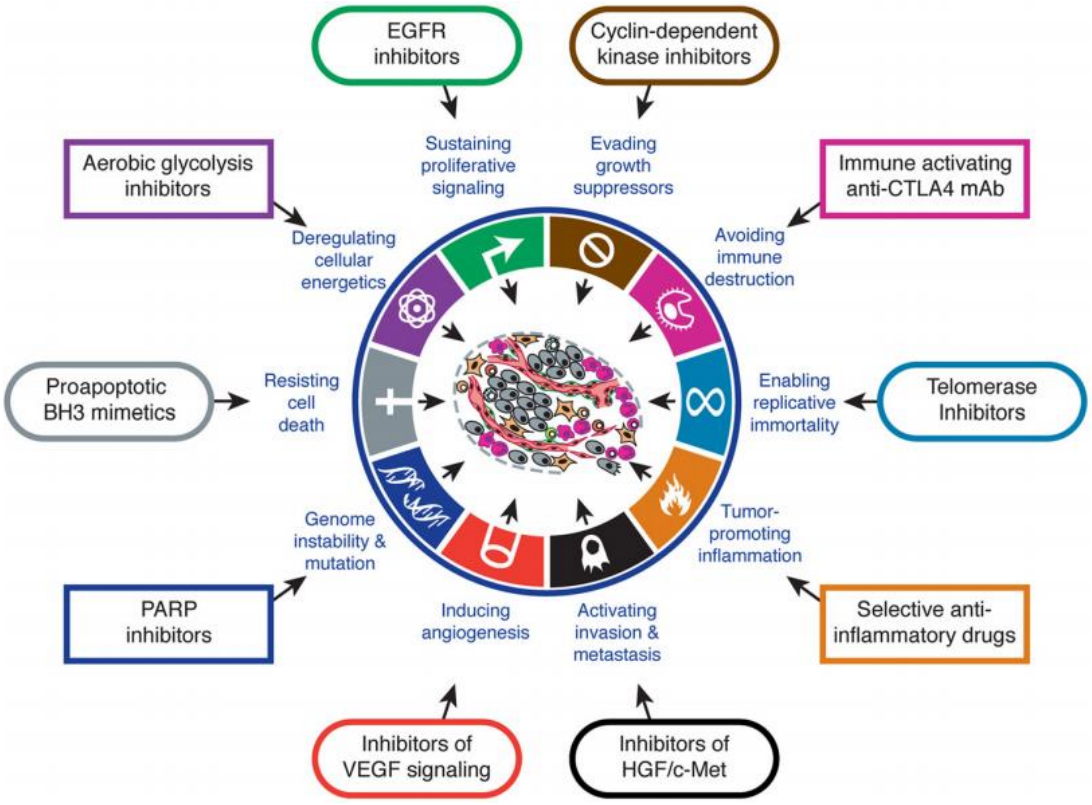

Figure 2 - Cancer cells hallmarks and examples of therapeutics that interfere with each of the acquired capabilities required for tumor growth and progression (adapted from (13)).

Another hallmark of cancer cells is their limitless replicative potential due to the overexpression of telomerase. This enzyme is a deoxyribonucleic acid (DNA) polymerase that adds repeated segments to the DNA ends. In normal cells, telomerase expression is almost absent, and with the successive replicative cycles, the capacity to conserve the telomeres (chromosomal ends of DNA) is impaired, which lead to cell death. However, with the overexpression of telomerase in cancer cells, the integrity of telomeres is maintained preventing DNA damage and cell apoptosis or senescence (13, 16). Additionally, cancer cells activate an angiogenic machinery through changes in the expression balance of angiogenic inducers and inhibitors. For example, angiopoietins, platelet-derived growth factors, fibroblast growth factor, and vascular endothelial growth factor are often overexpressed in the tumor tissue, promoting the formation of new vessels (8, 17-19). Therefore, cancer cells have access to a continuous supply of nutrients, oxygen, and means to dispose all the metabolic wastes. Moreover, cancer cells also develop an invasive phenotype by downregulating the expression of proteins involved in the cell-cell and cell-ECM adhesion (*e.g.* E-cadherin protein) and increasing the production of ECM-degrading enzymes, which in conjugation with a defective vasculature allow the cancer cells extravasation to blood circulation and tissue colonization (13, 20). More recently, it was demonstrated that cancer cells can avoid the recognition and destruction by the immune system and reprogram their metabolism (*e.g.* adjustments in the glycolytic pathways) to improve the tumor proliferation and progression (13).

1.1.3. Conventional therapies

Currently, there are several cancer treatments applied in the clinic that mainly include chemotherapy, radiotherapy, surgery, stem cell transplantation, and hormonal therapy (21). The combination of surgery with chemotherapy and/or radiotherapy is the most commonly used procedure to combat cancer. However, these therapies are not selective (damaging both cancer and healthy cells) and induce diverse side effects, which may spawn from nausea, fatigue, infertility, pain to organ failure or even death (21, 22).

The chemotherapy uses highly cytotoxic agents and is usually the first line of treatment for cancer therapy. However, the chemotherapeutic agents' therapeutic efficacy is limited by their low selectivity, rapid degradation, low water solubility, short half-life in blood circulation, and poor bioavailability (23, 24). Moreover, the cancer cells can acquire a multidrug resistance (MDR) phenotype, thus reducing the effectiveness of chemotherapy (25, 26). The mechanisms normally involved in MDR are: i) mutation in the drug target; ii) regulation of cell death mechanisms; iii) DNA damage repair; and iv) increase of membrane transporters that are involved in drug efflux. For example, the glycoprotein-P (P-gp) is a member of the ATP (adenosine triphosphate)-binding cassette transporters family, a group of transmembrane proteins that transport molecules to the exterior of the cell by the ATP hydrolysis (26, 27). This efflux pump is generally overexpressed on the membrane of cancer cells and their expression can also be further increased in response to the action of chemotherapeutics. Therefore, the P-gp avoids the intracellular accumulation of anti-cancer drugs impairing the drug action and decreasing their therapeutic effect (23, 28). Additionally, the acquisition of this MDR phenotype can also lead to the development of resistance to other chemotherapeutic agents, even those with distinct chemical structure. The MDR acquisition by cancer cells is nowadays one of the most serious problems associated with chemotherapy (24, 28, 29). Further, despite the advances in cancer chemotherapy, the shortcomings of the traditional approaches create a high demand for novel and more effective anti-cancer therapeutics.

1.2. Nanotechnology in cancer therapy

The recent breakthroughs in nanotechnology paved the way for a new era of anti-cancer medicines. The application of nanoparticles arises as one the most promising solutions to the problems faced by pharmaceutical industries in the development of more secure and efficient therapeutics (30, 31). Hence, in the last two decades, nanomedicines have been designed for improving the diagnosis, monitoring, and treatment of several diseases such as cancer (32, 33), Alzheimer (34, 35) and Parkinson (36, 37). In particular, the unique physicochemical properties of nano-sized platforms (1 to 1000 nm) and their capacity for transport and promote a specific delivery of drugs, prompted their application in cancer therapy, diagnosis, monitoring or in theragnostic applications (31, 38, 39).

1.2.1. Nanoparticles benefits for cancer treatments

When compared with conventional therapies, the utilization of nano-sized carriers has several benefits namely improved drug stability and solubility, protection against premature degradation, metabolism or even excretion. These factors improve the drugs half-life in the bloodstream improving their accumulation on tumor tissue and ultimately the therapeutic effect (39, 40). Furthermore, nanocarriers due to their reduced size and specific surface properties can take advantage of the tumor tissue architecture to preferentially accumulate and penetrate in the tumor tissue (41, 42). This nanoparticles accumulation occurs as a consequence of the enhanced permeability and retention (EPR) effect. The EPR effect is based on the leaky vasculature of the tumor blood vessels that display fenestrae with 400 to 600 nm, that allow nanoparticles to escape from blood circulation. Further, the tumor tissue also presents an impaired lymphatic drainage, which favors the nanoparticles' retention (19). Besides this passive targeting, nanoparticles can also contain targeting moieties that exploit ligand-receptor, antigen-antibody, and other forms of molecular recognition with molecules uniquely expressed or overexpressed in tumor cells for enhancing its accumulation in this tissue (42-44). Beyond the improved biodistribution, nanoparticles can be engineered to release and deliver their cargo in a spatial-temporal controlled way, improving the amount of drug that reaches the tumor tissue, while simultaneously avoiding the drug interactions with healthy tissues. The nanoparticles can release their content in response to local or external stimuli, such as electromagnetic field, near-infrared (NIR) radiation, pH, and ultrasound (Figure 3). Thus, these nanoparticle features can further contribute to the reduction of chemotherapy side effects (38, 45, 46).

1.2.2. Nanoparticles for drug delivery: the main properties

The administration of drug delivery systems in the human body can be performed by different routes, being the intravenous procedure the most commonly used. Once inside the bloodstream nanoparticles must remain stable to avoid their aggregation or degradation (*e.g.* oxidation or hydrolysis) (47-50). Further, nanoparticles must evade the clearance by renal filtration and the uptake by the reticuloendothelial system (RES) organs (liver and spleen) that can entrap and degrade nanoparticles. Additionally, nanoparticles should be able to dodge the adsorption of plasma proteins (*e.g.* serum albumin, complement components, and immunoglobulins) to their surface, since the adsorbed proteins can be recognized by phagocytic cells, leading to the nanoparticles clearance (50-52). After reaching the tumor zone, nanoparticles must be able to extravasate from the tumor vessels into the tumor tissue, in a concentration that guarantees the therapeutic effect. The nanoparticles extravasation is largely influenced by the abnormal and leaky tumor vasculature and by the impaired lymphatic drainage (EPR effect) (42, 50, 52).

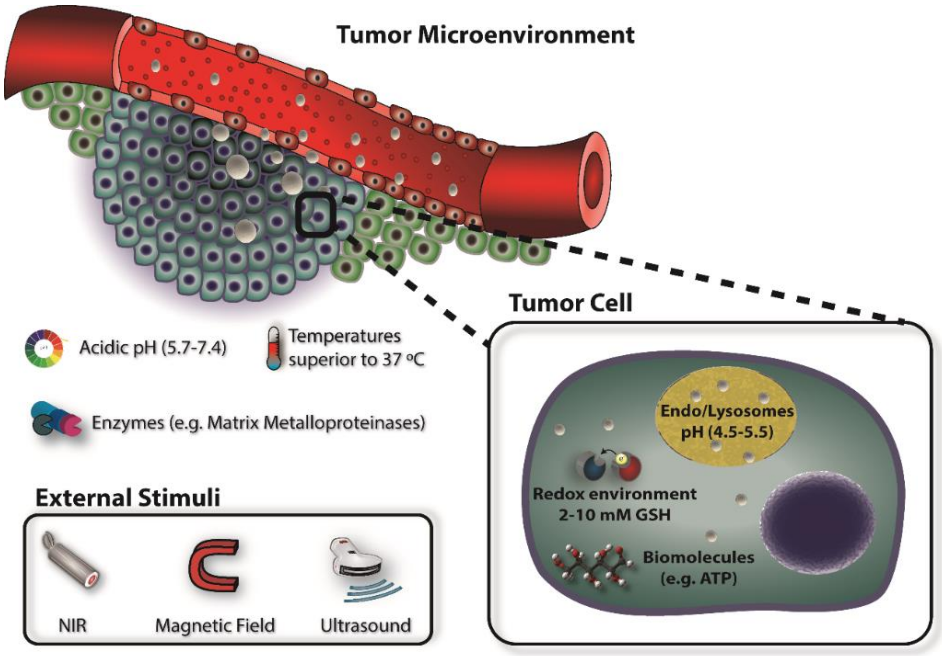

Figure 3 - Schematic representation of the nanoparticles extravasation in the tumor vasculature (EPR effect) and the different stimuli that can trigger the release of the agents encapsulated by the nanoparticles. The triggered drug release circumvent the drug interaction with healthy tissues and improve the therapeutic effect (adapted from (38)).

Subsequently, the nanoparticles must penetrate through the tumor mass to reach the cancer cells. This process is impaired by the dense ECM and high interstitial fluid pressure that is found in tumors, thus preventing the nanovehicles penetration into deeper regions of the tumor and, also causing a heterogeneous nanoparticle distribution. Lastly, the nanosystems should be internalized by cancer cells and release their content in the intracellular compartment (19, 50, 53).

For a successful nanoparticle-mediated therapy, these nanoplatforms must be carefully designed to display a specific size, morphology, charge, and corona composition (Figure 4) (42, 54). These parameters influence the particle interaction with the human body and their pharmacokinetic profile, which ultimately determine the dose of therapeutic agents delivered into the tumor and thus the therapeutic outcome (53).

1.2.2.1. Nanoparticles size

During the nanoparticle design, researchers have to consider several size limits (Figure 5). For example, particles with sizes inferior to 5 nm are rapidly eliminated by renal filtration. Moreover, the size also regulates the nanoparticles filtration and uptake by the RES. Nanoparticle with sizes lower than 50 nm can interact with hepatocytes (extravasate through the liver fenestrations (50 –100 nm)), whereas nanoparticles larger than 200 nm accumulate in the spleen. Moreover, larger nanoparticles are also sequestered by the macrophages residing

in liver and spleen. Considering these size limits and those imposed by the EPR effect, the ideal nanoparticle size should be comprehended between 100 and 200 nm (19, 51, 55).

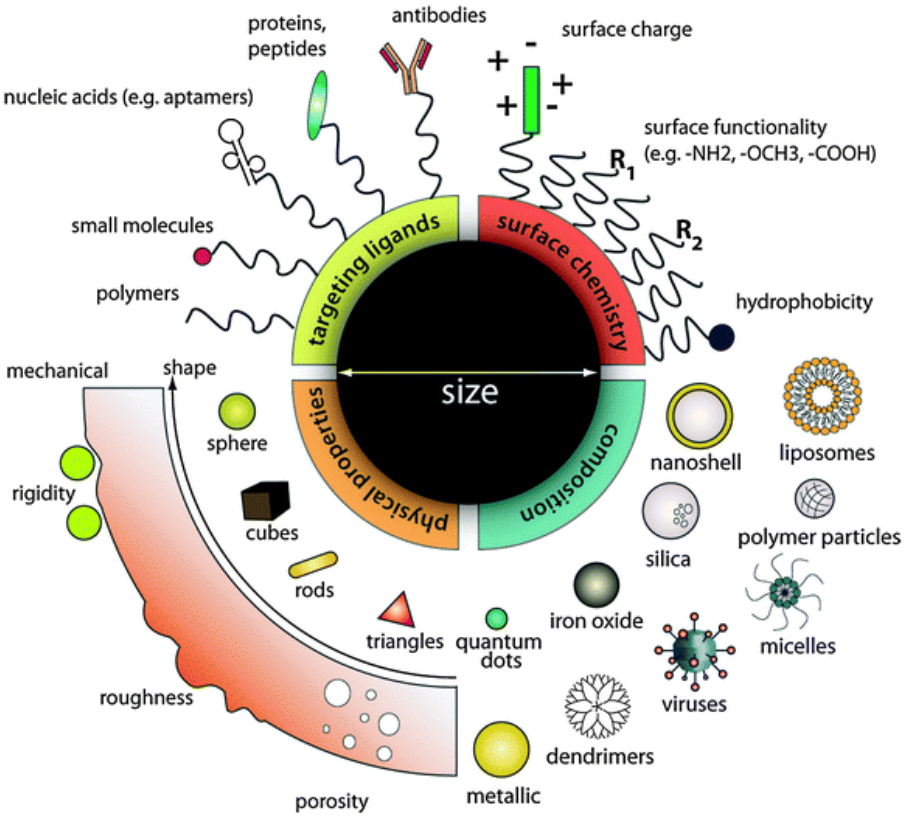

Figure 4 - Overview of nanoparticles physicochemical properties. The nanoparticles size, morphology, charge, surface chemistry, and composition play a major role in their biological performance and interaction with the human body (adapted from (54)).

The nanoparticles size also influences their tumor penetration. In general, bigger nanoparticles have a low tumor penetration capacity, whereas the smaller ones are more prone to penetrate deeper and faster in the tumor mass. Finally, nanoparticles cellular internalization is also affected by their size (19, 51). Small nanoparticles (4-10 nm) can become internalized in cancer cells by direct transposition of the lipid bilayer membrane (56). On the other hand, bigger nanoparticles are internalized by pinocytosis, in a process comprising clathrin-dependent endocytosis (~120 nm, destined to lysosomes) or clathrin-independent endocytosis. The latter pathway encompasses the caveolin-dependent endocytosis (~60 nm), clathrin-and caveolin-independent endocytosis (~120 nm), and macropinocytosis (>1 μm). In this way, size affects the fate of internalized nanoparticles since some uptake routes direct the nanoparticles to the lysosomes, which can lead to the degradation of the loaded cargo by hydrolytic mechanisms (19, 38, 57).

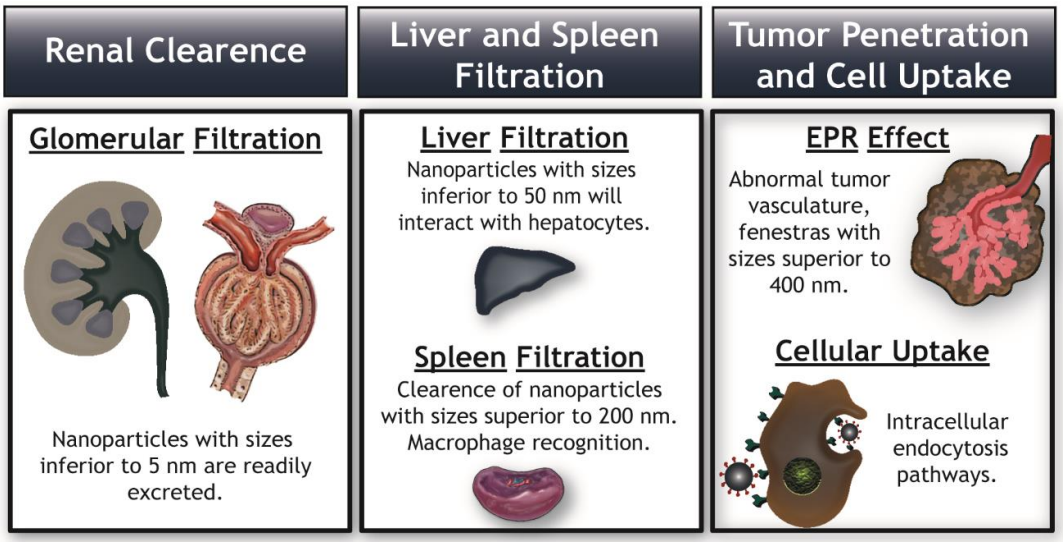

Figure 5 - Representation of the barriers that the nanoparticles have to overcome during blood circulation. Nanoparticles must avoid the renal, liver, and spleen clearance, extravasate through tumor vasculature and interact with cancer cells (adapted from(38)).

1.2.2.2. Nanoparticles composition

The nanoparticles surface composition plays an important role in the nanovehicles biodistribution. Nanoparticles surface can be functionalized with hydrophilic polymers to improve their solubility and stability. The most commonly adopted polymer to achieve such properties is polyethylene glycol (PEG). PEG coatings can also reduce nanoparticles opsonization, protect them from degradation and reduce their uptake by macrophages (19, 58).

However, the properties conferred by this type of coating are dependent on factors, such as PEG density and molecular weight. Recently, some research groups have demonstrated that anti-PEG antibodies are produced after injection of PEGylated nanomaterials, which leads to the rapid elimination of nanoparticles in the subsequent administrations –a phenomenon termed Accelerated Blood Clearance (59, 60). Due to that, other types of coatings are being investigated, such as polyoxazolines (PEOZ) and poly(glycerol) acid (PGA) (61, 62). On the other side, inorganic materials have also been used for coating the nanomaterials surface. These inorganic materials can increase the nanoparticles solubility, protect their internal structure from degradation and confer thermal and chemical stability (46, 63). Moreover, nanoparticles surface can also be grafted with targeting ligands (*e.g.* folic acid and antibodies, to improve their selectivity towards cancer cells) (42, 44).

1.2.2.3. Nanoparticles charge

The nanoparticles charge affects their circulation time in the bloodstream. In fact, nanoparticles displaying highly positive surface charges (*i.e.* zeta potential > +10 mV) will interact with blood proteins, leading to their opsonization and clearance, whereas negatively charged nanovehicles (*i.e.* zeta potential < -10 mV) will be uptaken by RES. Thereby, a neutral

charge (±10 mV) is often considered ideal for nanoparticles, being less prone to suffer opsonization and RES uptake (19, 42). Additionality, nanoparticles charge may impair their tumor penetration by interacting with the charged components of the tumor ECM. Positively charged particles tend to interact with hyaluronic acid, while those with a negatively charged surface interact with collagen. Thus, neutrally charged nanoparticles are also the most appropriated for penetrating deeper into the tumor mass (19, 40).

1.2.2.4. Nanoparticles shape

The contribution of nanoparticles shape on their interaction with the human body has not been yet fully characterized, and it is also a subject of strong debate since the data available in the literature is often contradictory. For example, there is some controversy in the literature about the shape effect on the nanomaterials capacity to reach the tumor zone. Janát-Amsburyet and co-workers verified that PEGylated gold nanorods achieve a higher tumor accumulation than gold nanospheres, most likely due to their longer blood circulation time and lower uptake by the liver and spleen (64). In another work, Black and co-workers reported that PEGylated gold nanospheres presented the highest tumor accumulation, followed by nanocages, nanodisks, and nanorods. In this report, the spherical nanoparticles also displayed a higher blood circulation time and a lower RES organ uptake than the other structures, leading to their higher tumor accumulation. Moreover, it was also observed that elongate-shaped materials are more difficult to remove from the tumor site than those spherically shaped. In addition, the nanoparticles shape also affects the particles penetration and distribution within the tumor tissue. Black and colleagues observed that gold nanorods and nanocages presented a wider tumor distribution, whereas the nanospheres and nanodisks were mainly confined to the tumor periphery (19, 51, 65). Moreover, the effect of the nanoparticle shape on the cellular uptake appear to be material dependent, *i.e.*, silica and iron oxide non-spherical nanocarriers present an enhanced cellular internalization, while for polymers and gold, the spherical shaped particles are the ones that present the better cellular internalization (19, 65). Finally, during blood circulation, the nanoparticle shape will affect their interaction with the macrophages and consequently impact on the nanoparticle circulation time (19, 56, 66). For instance, worm-like and rod-shaped nanocarriers are less phagocytized than the spherical-shaped ones (64, 67).

1.3. Gold nanoparticles

The controlled drug delivery mediated by nanoparticles has progressed over the years, as well as the nanoparticles requirement to be applied in the clinic. Each type of nanoparticles has specific characteristics that enable their utilization in cancer therapy. Currently, nanoparticles can be classified into two main classes: organic and inorganic nanoparticles. Organic nanoparticles are produced with natural or synthetic compounds and comprise polymer-based nanocarriers (micelles and dendrimers) and lipid-based nanocarriers (liposomes and solid-lipid nanoparticles) (68). Despite liposomal- and micelle-based nanoparticles present nowadays a wide dissemination in clinical practice (69), inorganic nanoparticles also possess exciting

properties that can prompt their utilization in the clinic (70, 71). This class, comprise magnetic nanoparticles, carbon nanotubes, quantum dots, silica, and gold nanoparticles that are associated with a higher inertness, stability, and resistance to degradation. Further, their intrinsic optical, magnetic, photothermal, and electronic properties can be adapted by controlling their crystal phase, size, shape, and surface characteristics originating multifunctional nanomedicines for cancer therapy and imaging (68, 72).

1.3.1. General properties of gold nanoparticles

Among the wide variety of inorganic nanoparticles reported in the literature, gold nanoparticles assume an increased relevance when biomedical applications are envisioned. Gold is one of the least reactive known metals and presents resistance against oxidation and corrosion (73). Further, gold nanoparticles present unique optical properties, due to the surface plasmon resonance phenomenon (*i.e.* the light scattering or absorption in response to the free electrons synchronized oscillation when the particle is exposed to light at their resonance wavelength). The production of gold nanoparticles with different shapes (*e.g.* rods, cubes, triangles, cages, stars or others) has allowed the tuning of the particles' resonance wavelength to the near infra-red (NIR) region, a radiation range where the human body components present almost no absorption (reviewed in detail by (74-77)). This control over gold nanoparticles surface plasmon resonance has been exploited to apply them as bioimaging and/or photothermal agents (78-83).

Despite the wide scope of applications of gold nanostructures, they also display some limitations that can impair their utilization in biological systems. Gold nanoparticles can interact with compounds containing thiol or disulfide groups through the formation of relatively strong gold-thiolate bonds (84). This well-known gold binding affinity or the establishment of non-specific interactions trigger the biomolecules adsorption on the nanoparticles' surface (85, 86). Particularly, the adsorption of proteins can induce changes on the nanoparticles' surface properties and thus on their interaction with the human body (*e.g.* nanoparticles uptake, blood circulation time and biocompatibility) (87, 88). Moreover, gold nanoparticles during bioimaging or therapeutic applications can be exposed to high-energy laser pulses and a portion of the incident radiation is converted into heat (89). In turn, the generated heat can lead to the gold nanoparticle reshaping (*i.e.* melting) and consequently loss of their optical properties (74, 90). Therefore, the post-synthesis modification of gold nanoparticles is highly desirable for surpassing these limitations as well as potentiate gold-based nanoparticles application in nanomedicine (91-93). From the wide number of materials used in the literature (*e.g.* dextran, poly(isobutylene-alt-maleic anhydride)-graft-dodecyl and PEG), silica arises as one of the main coating alternatives for gold nanoparticles (94, 95).

1.3.2. Gold core-silica shell nanoparticles

Nanoparticles produced with silica have been reported as stable colloidal suspensions, chemically inert, biocompatible and simple to modify with different functional groups (96, 97). Further, silica derivatives such as mesoporous silica possess a large surface area and pores that can act as reservoirs for bioactive molecules aimed for therapeutic purposes (32, 97). Such features allow the encapsulation of poorly soluble compounds and simultaneously confer them protection from premature degradation and clearance from the human body (98, 99). In addition, the inclusion of the silica shell also enhances the colloidal stability of gold nanoparticles when they are in contact with biological fluids or irradiated with a specific radiation (100, 101). Silica is also optically transparent to the NIR radiation, often used in photothermal therapy (PTT), which indicates that the silica shell does not compromise the therapeutic capacity of gold-based PTT agents (102, 103). Therefore, the multifunctional potential of gold core-silica coated (Au-MSS) nanoparticles provides an ideal platform for theragnostic modalities combining therapeutic, targeting, and imaging functions (please see Figure 6).

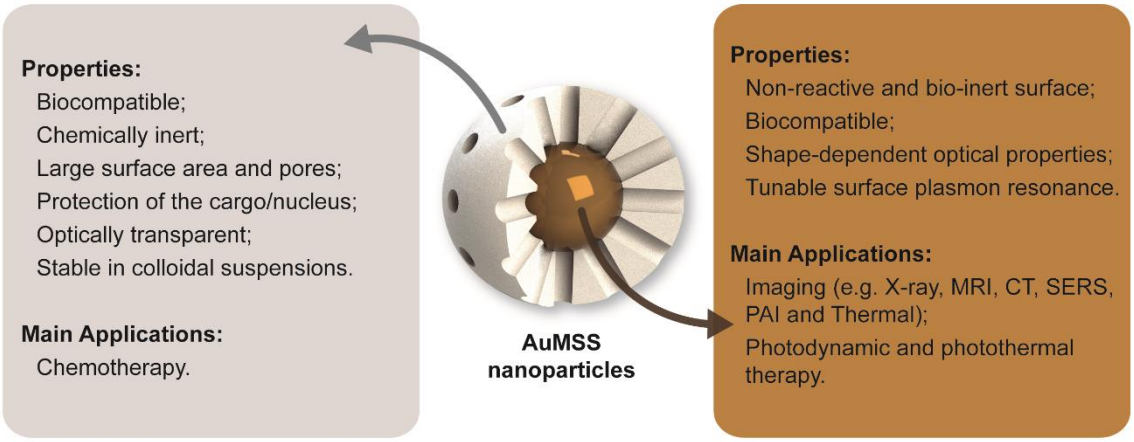

Figure 6 - General properties and main applications of the Au-MSS materials. The gold core allows the particle application in bioimaging and PTT. The inclusion of the silica shell stabilizes the gold core and improves drug delivery capacity of the nanoparticles.

During the past years, a huge effort has been performed to allow the fabrication of Au-MSS nanoparticles in a scalable, controlled and reproducible manner (104-106). Generally, the production of these nanoparticles can be achieved through two main steps (please see Figure 7), i) the production of the gold core with the desired size and shape and ii) the synthesis of the silica shell (105, 107, 108). The gold cores can be synthesized using different synthetic routes to yield gold nanoparticles with distinct sizes and shapes, as extensively reviewed in (75, 109-111).

Briefly, gold cores are usually prepared by inducing the reduction of gold salts and consequent gold nucleation and growth in the presence of a stabilizing agent, such as trisodium citrate and

cetyltrimethylammonium bromide (CTAB), to prevent the particles aggregation (109). The sphere is one of the most stable shapes and can be obtained when the gold core synthesis is performed under thermodynamically controlled conditions (112). Alternatively, to obtain non-spherical gold-cores the synthesis process must be fine-tuned to favor an anisotropic growth of the gold core by using surfactants that block some of the growing directions (*e.g.* CTAB (113, 114), halides (115, 116) or weak/mild reduction agents (117, 118). Up to date, the rod-like shape remains as one of the most explored gold nanostructures. In general, gold nanorods are produced by using a seed-mediated growth methodology (108, 119), where small spherical gold spheres (*i.e.* seeds) are synthesized by nucleation and then they are added to a solution denominated of "growth solution", which is composed of a gold salt (*e.g.* chloroauric acid), silver nitrate and high concentrations of CTAB to induce the rod-shaped growth (119). Gold nanostars and nanocages have also been used for biomedical applications. Gold nanostars are also produced by using a seed-mediated growth method, however, the particle growth occurs in the surface of poly(vinyl pyrrolidone) coated gold seeds in the presence of dimethylformamide (120). On the other hand, gold nanocages are prepared by using sacrificial silver nanocubes which are exchanged by gold through a galvanic replacement process (121).

Subsequently, the silica coating of the gold cores is accomplished by using the classic Stöber method or its derivations (105, 106). During the synthesis procedure, the silica precursor (*e.g.* tetraethyl orthosilicate (TEOS)) molecules will start to condensate around the gold core originating the silica shell. The thickness of this silica shell can be tailored by fine-tuning the reaction time and reagent concentrations (105). In these systems, the optical and electronic properties can be adjusted by varying the shape and size of the gold core as well as the thickness of the silica shell (122, 123). On the other side, the silica coating allows the stabilization of the gold nanostructures as well as the encapsulation of drugs, dye molecules, or other imaging agents either via physical adsorption or covalent attachment (38, 124). Further, silica presents an increased surface area that can be functionalized with antibodies, targeting moieties or even stealth agents (38, 99). Therefore, Au-MSS nanoparticles with different core shapes (*i.e.* spheres, rods, stars, and cages) have been employed, in different reports in the literature, for therapeutic and bioimaging applications (125-127). Au-MSS nanoparticles have been explored to mediate single or combinatorial therapeutic approaches based on drug delivery, PTT and photodynamic therapy (PDT) (83, 128-131). The possibility to combine different therapeutic functions into one nanoparticle presents benefits, since it improves the therapeutic efficacy, due to possible synergic interactions, and minimizes the side-effects originated by the administration of multiple doses (39, 132). Further, the gold-core allows the realization of bioimaging techniques such as computerized tomography (CT), magnetic resonance imaging (MRI), photoacoustic (PA) imaging and surface enhanced Raman spectroscopy (SERS) (133, 134).

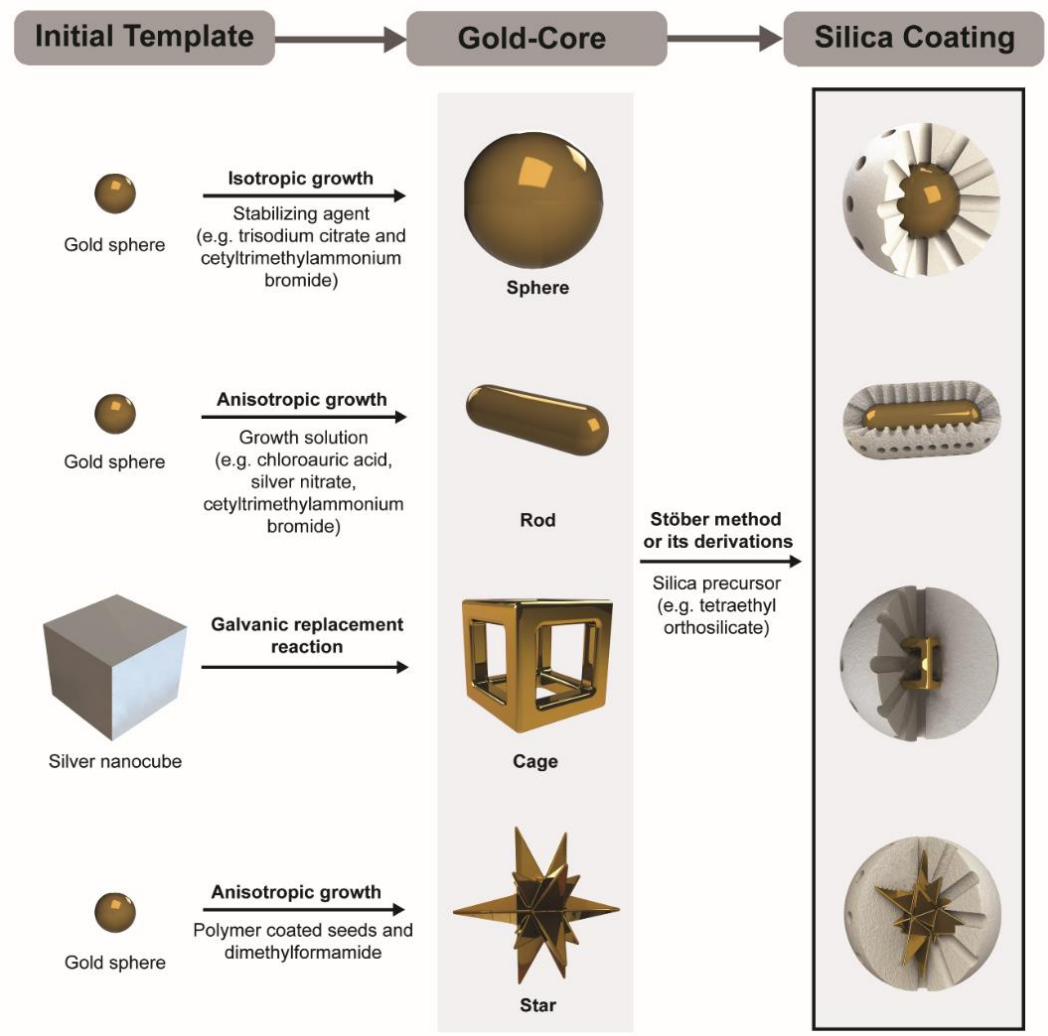

Figure 7 - Representation of Au-MSS production process. The production of the gold-core is achieved by promoting an isotropic or anisotropic growth or by using sacrificial templates. Afterward, the gold-core with the desired shape is coated with a silica layer by using the Stöber method or its derivations.

1.3.2.1. Au-MSS nanoparticles biocompatibility

The application of Au-MSS nanoparticles in the clinic is closely connected to the complete understanding of the nanoparticles-host interactions that occur upon administration. Therefore, several extensive *in vitro* and *in vivo* toxicological evaluations must be performed using different Au-MSS systems and cell or animal models, before they can be tested in clinical trials. Zeng and colleagues observed that the cytotoxicity of Au-MSS nanospheres is size and dose-dependent (135). They verified that Au-MSS nanospheres with 50, 100 and 200 nm silica layers did not induce any significant cytotoxicity in concentrations inferior to 200 pmol/L, whereas when the concentration was increased to 400 pmol/L, the spheres with 200 nm silica layer decreased the Liver hepatocellular carcinoma (HepG2) cell viability in 10 %. In another work, Dias and colleagues compared the cytotoxicity of spherical and rod-like Au-MSS nanoparticles (46). The administration of both spherical and rod-like nanoparticles to Human

negroid cervix epithelioid carcinoma (HeLa) cells and human fibroblasts revealed that both systems were biocompatible up to 100 μg/mL. Moreover, the authors observed that the rod-like nanoparticles exerted a positive effect on the cell migration capacity, presenting a gap with a smaller width than the cells treated with the spherical Au-MSS in the *in vitro* wound closure assays.

Apart from the acute toxicity of the Au-MSS nanoparticles, the systemic toxicity and distribution greatly impact the biological performance of the nanoparticles. Thakor *et al*. studied the systemic biodistribution and acute effects of PEGylated Au-MSS nanospheres (size 120 nm) administered via intravenous administration in mice (136). Their initial results demonstrated that the particles did not affect the physical appearance, behavior or social interactions in any of the mice studied, neither induce any acute effects on basal cardiovascular function and on hematological and biochemical parameters recorded. Furthermore, the authors found out that the PEGylated Au-MSS nanospheres accumulate mainly on liver and spleen, which induced a mild inflammatory response in the liver through reactive oxygen species formation at 24 h post-administration, but not detected 1 week after injection. In turn, Gao *et al*. evaluated the biocompatibility and biodistribution of folic acid functionalized Au-MSS nanorods in rabbits (137). In their study, particles concentration up to 40 ppm did not elicit any significant cytotoxic effect on HepG2 cells. Further, the folic acid functionalized Au-MSS displayed a preferential accumulation in the tumor tissues and started to be cleared from the body after 24 h through the kidneys. Moreover, no serious signs of toxicity in vital organs were observed by the authors even when high doses (10.5 mg/kg) were administered.

Despite, to rationally apply Au-MSS nanoparticles in the clinic it is still necessary to perform additional studies, such as the characterization of the Au-MSS particle shape and administration route influence on the particles performance, to better understand the Au-MSS particles behavior in biological environments.

1.3.2.2. Rod-like shape

The rod-like shaped nanoparticles are the most explored Au-MSS particles when therapeutic applications are intended. This increased interest on the Au-MSS nanorods is based on their tunable optical properties and effective light-heat conversion (76, 88). The Au-MSS nanorods present two distinct absorption peaks that correspond to the transverse and longitudinal resonances (76). The transverse resonance leads to an absorption peak at 520 nm, whereas the longitudinal resonance can be easily tuned to present high absorption in the NIR region, through the simple manipulation of the rod aspect ratio (AR), *i.e*. rod length/width coefficient (138). These important characteristics favor the Au-MSS nanorods application in imaging (PA and X-ray) and therapy (*e.g*. chemotherapy, PTT, PDT or their combination (139-141)). The PA imaging takes advantage of the ultrasounds generated by the temperature increase and consequent rapid pressure differences created by NIR laser irradiation of Au-MSS nanorods

(133). Cheng *et al*. demonstrated that Au-MSS nanorods present an increased stability when compared to bare and PEGylated gold nanorods, for being applied in PA imaging (89). The extra protection provided by the silica shell (*i.e*. thickness 6 nm or 20 nm) resulted in the stabilization of the PA signal during 300 pulses. In contrast, the signal of PEGylated gold nanorods decreased 40 % in the first 100 pulses. Further, they also observed that the inclusion of the 20 nm silica shell increases the amplitude of the PA signal generated by the gold nanorods, which can lead to clear and better images (89).

Apart from imaging, the Au-MSS nanorods capacity to absorb radiation in the NIR region have also been explored to mediate therapeutic applications, mainly in cancer PTT (142, 143). Liu *et al*. developed a tLyp-1 peptide-functionalized, indocyanine green-loaded Au-MSS nanorods for the breast cancer PTT and indocyanine green-mediated imaging (144). The nanorods had an AR of 3.5 (length 47 nm and width 14 nm) with a 17-32 nm silica shell and presented a strong absorption peak in the NIR region, at 754 nm. Further, the nanoparticles mediated an increase in the temperature up to 55 ºC and a decrease in MDA-MB-231 cells viability to values inferior to 20 %, when irradiated with a NIR laser (785 nm, 3 $W.cm^{-2}$ for 2 min). Similarly, Lee *et al*. developed an RVG29 (29 residue peptide derived from rabies virus glycoprotein) functionalized Au-MSS nanorods for the PTT of brain gliomas (145). The produced Au-MSS nanorods had an AR of 2.4 (length 180 nm, width 75 nm, and 14 nm shell thickness) and presented high absorption in the NIR region. The RVG29 functionalization of the Au-MSS nanorods proved to be capable of increasing the nanoparticles accumulation in the brain region of glioma-bearing mice. Further, the nanoparticles NIR laser irradiation (808 nm, 5 min, and 1.5 $W.cm^{-2}$) increased the local tumor temperature to values around the 50 ºC, thus suppressing the growth of the xenografted tumor and allowed the real-time monitoring via MRI during the 7 days, the total duration of the study (145).

However, the Au-MSS-mediated PTT is hindered by light scattering and absorption phenomena that occur when the NIR light travels deeper into the tissues (146, 147). Therefore, depending on tumor location, some cells will inevitably receive suboptimal laser exposure and survive (146, 147). With that in mind, several studies have been combining the Au-MSS-mediated PTT with chemotherapy or PDT to improve the therapeutic outcome (130, 148). Shen and colleagues produced doxorubicin hydrochloride (Dox) loaded Au-MSS nanorods functionalized with Arginylglycylaspartic acid (RGD) moieties for the targeted chemo- and PTT combinatorial therapy (149). The particles presented an AR 3.9 (length 52 nm, width 13 nm, and 25 nm shell thickness), strong absorption in the NIR wavelength region (absorption peak at 840 nm) and a drug release that could be induced by the NIR laser irradiation and consequent heat generation. Additionally, the nanoparticles intravenous administration in human lung carcinoma (A549) tumor-bearing mice shown that the nanoparticles could mediate an increase in the tumor temperature up to 65.9 ºC after NIR laser irradiation (808 nm, 30 seconds and 3 $W.cm^{-2}$). In addition, the anti-tumoral efficiency of the nanorods was enhanced when chemo and thermal

therapies were combined, being registered a tumor weight inhibition rate of 66.5 % and 45.2 % for the combinatorial therapy and single PTT therapy, respectively.

Recently, Zhou *et al*. developed hyaluronic acid and RGD peptide functionalized Au-MSS nanorods loaded with Dox for the combinatorial therapy of ovarian cancer. The nanorods (length 50 nm, width 10 nm, and shell thickness of 15 nm) irradiation with NIR laser (808 nm, 2 $W.cm^{-2}$ and 4 min) resulted in an improved therapeutic effect towards ovarian SKOV-3 cancer cells (10 %, 29 % and 46.5 % cell viability for combinatorial, chemotherapy and PTT, respectively) (143). With a different approach, Moreira and colleagues encapsulated Au-MSS nanorods loaded with Dox within poly (lactic-co-glycolic acid) based microparticles containing salicylic acid for the chemotherapy and PTT combinatorial therapy of cervical cancer (45). The authors observed that the heat generated by the nanorods irradiation with a NIR laser (808 nm, 1.7 $W.cm^{-2}$ and 5 min) could trigger the drug release and enhance the particles cytotoxicity, *i.e*. the cell viability within HeLa spheroids was reduced to 25 %, when spheroids were irradiated with NIR laser, whereas in the non-irradiated group, 50 % of the cells remained viable. On the other side, Seo *et al*. explored the combination of the PTT and PDT by using Au-MSS nanorods (length 32 nm, width 11 nm, and shell thickness 20 nm) loaded with methylene blue (150). Upon NIR laser irradiation (780 nm, 1 $W.cm^{-2}$), the authors observed a synergistic effect between the heat generated by the nanorods and the reactive oxygen species created by the methylene blue molecules leading to a decrease in the cell viability to 11 %. Moreover, these nanoparticles also allowed the detection of both agglomerated and single cancer cells through SERS imaging. In an integrative study, Luo and colleagues developed cisplatin and $AlPcS_4$ loaded Au-MSS nanorods functionalized with ß-cyclodextrins, adamantine conjugated poly(ethylene glycol) and lactobionic acid for the simultaneous PTT, PDT, and chemotherapy of hepatic cancer (151). The intravenous administration of Au-MSS nanorods (length 40 nm, width 10 nm, and shell thickness 14 nm) triple therapy in HepG2 tumor-bearing mice increased the tumors local temperature to 53 ºC and ceased the tumor progression upon irradiation with NIR laser (808 nm and 606 nm, 1 $W.cm^{-2}$ for 5 min). In sharp contrast, the tumor continued to progress when only PTT/chemotherapy (4-fold volume increase) or PDT/chemotherapy (4.9-fold volume increase) were used.

In general, during the past years, the practical research developed in these field has been focused on the improvement of the nanoparticles circulation time and control of the drug release profile. These characteristics will improve the nanoparticles probability to accumulate in the tumor tissue, while simultaneously decreasing the chemotherapeutics interaction with healthy tissues, which ultimately enhance the therapeutic effect.

Aims

The main goal of this dissertation was to design and develop a novel Au-MSS surface modification based on biofunctional polymers for overcoming the uncontrolled release profile, limited blood circulation and ultimately potentiate the therapeutic effect. For that purpose, two different methodologies, electrostatic interaction or chemical linkage, were explored and optimized to functionalize Au-MSS nanoparticles with a rod-like shape with D-α tocopherol polyethylene glycol 1000 succinate (TPGS) and branched polyethyleneimine (PEI), originating the Au-MSS/TPGS-PEI and Au-MSS/TPGS/PEI formulations.

Therefore, the specific objectives include:

- → Synthesis, purification, and characterization of Au-MSS nanorods;
- → Synthesis of TPGS-PEI, TESPIC-TPGS, and TESPIC-PEI polymers;
- → Functionalization of Au-MSS and characterization of the nanocarriers' physicochemical properties;
- → Evaluation of the Au-MSS formulations drug loading capacity;
- → Evaluation of the photothermal capacity;
- → Evaluation of the Au-MSS formulations biocompatibility;
- → Evaluation of the nanoparticles' cellular uptake.

Chapter 2

Materials and Methods

2. Materials and Methods

2.1. Materials

Hydrogen tetrachloroaurate (III) hydrate ($HAuCl_4$) was purchased from Alfa Aesar (Karlsruhe, Germany). TEOS and tetrahydrofuran (THF) were obtained from Acros Organics (Geel, Belgium). CTAB was acquired from Tokyo Chemical Industry (Tokyo, Japan). Hydrochloric acid (HCl) was purchased to Panreac (Barcelona, Spain). Methanol was obtained from VWR International (Carnaxide, Portugal). Sodium Hydroxide (NaOH) was purchased from Labkem (Barcelona, Spain). Dulbecco's Modified Eagle medium-high glucose (DMEM-HG), Ethanol (EtOH), Fluorescein 5-isothiocyanate (FITC), L-ascorbic acid (AA), Paraformaldehyde, PEI (Mw~1250 g/mol, ρ=1.08 g/mL), Phosphate-buffered saline (PBS) solution, Resazurin, Silver nitrate ($AgNO_3$), Sodium borohydride ($NaBH_4$), Toluene, TPGS, Trypsin, 1,1'-Carbonyldiimidazole (CDI) and 3-(Triethoxysilyl)propyl isocyanate (TESPIC) were bought from Sigma-Aldrich (Sintra, Portugal). HeLa cells (ATCCs CCL-2t) were acquired from ATCC (Middlesex, United Kingdom (UK)). Fetal bovine serum (FBS) was acquired to Biochrom AG (Berlin, Germany). Wheat germ agglutinin conjugate Alexa 594® (WGA-Alexa Fluor 594®) and Hoechst 33342® were purchased from Invitrogen (Carlsbad). Dox was obtained from Carbosynth (Berkshire, UK). Cell imaging plates were acquired from Ibidi GmbH (Ibidi, Munich, Germany). Cell culture t-flasks were supplied by Orange Scientific (Braine-l'Alleud, Belgium).

2.2. Methods

2.2.1. Synthesis of Au-MSS Rods

The nanorods were synthesized through a method comprised of 3 main steps, as previously described in the literature (45, 152, 153). In the first step, a seed solution was prepared through the addition of 0.6 mL of $NaBH_4$ (0.01 M) under magnetic stirring, to an aqueous solution with 5 mL of CTAB (0.2 M) and 5 mL of $HAuCl_4$ (0.0005 M). After 6 hours at 30 ºC, the seed solution was added to a growth solution, which was prepared by adding under magnetic stirring 0.03 mL of $AgNO_3$ (0.1 M), 0.3 mL of $HAuCl_4$ (0.05 M) and 0.21 mL of AA (0.08 M) to an aqueous solution containing 20 mL of CTAB (0.2 M). The resulting solution was left undisturbed for 16 h, at 30 ºC, to promote the formation of gold nanorods.

The synthesis of mesoporous silica shell was carried out by adapting the method described by Dias and co-workers (46). Initially, the gold nanorods were centrifuged (12,000g, for 20 min at 25 ºC) to remove the excess of CTAB and resuspended in ultrapure water. Then, 0.7 mL of CTAB (0.01 M) was added and left under stirring overnight at 40 ºC. Afterward, 0.07 mL of NaOH (0.1 M) was added to the solution, mixed over 30 min and 0.03 mL of a solution of TEOS (20 % v/v) in methanol were added. The TEOS addition was repeated three times, with 30 min intervals, and the solution was left under stirring for 24 h at 40 ºC. The final solution was

centrifuged (12,000g, for 25 min at 25 ºC) and washed with ultrapure water in order to recover the Au-MSS nanorods.

2.2.2. Removal of the surfactant template

The surfactant removal (CTAB) from Au-MSS nanorods was performed through a solvent based approach described in the literature (32). Briefly, the nanoparticles were resuspended in an acidic solution (HCl 5 % v/v in EtOH), sonicated for 2 min, and centrifuged (18,000g for 15 min at 4 ºC). This step was repeated several times, followed by two washing cycles with EtOH (99.9 % v/v) and ultrapure water. The final product was recovered by centrifugation and resuspended in ultrapure water.

2.2.3. Synthesis of TPGS-PEI co-polymer and TESPIC-TPGS and TESPIC-PEI derivatives

TPGS-PEI co-polymer was synthesized through a method previously described elsewhere (154, 155). Briefly, TPGS (100 mg) was dissolved in 20 mL of anhydrous toluene, under a nitrogen atmosphere, for 6 h at room temperature. Then TPGS was activated with CDI (24 mg) and mixed over 24 h, under a nitrogen atmosphere. Afterward, PEI (0.1 mL) was added to the activated TPGS and left under stirring for 24 h. After the reaction time, the solvent was evaporated (Rotavap®R-215, Büchi, Switzerland) and the remaining film was hydrated with ultrapure water, sonicated, dialyzed and recovered by freeze-drying. In order to allow the chemical linkage of TPGS and PEI to the Au-MSS nanorods, the polymers were individually modified with TESPIC by adapting a method previously described in the literature (156, 157). Briefly, TPGS (500 mg) or PEI (0.1 mL) were dissolved in 20 mL of anhydrous THF under a nitrogen atmosphere and magnetic stirring, for 6 h at room temperature. Subsequently, TESPIC was added to the polymer solution and left to react for 24 h. Thereafter, the solvent was evaporated (Rotavap®R-215, Büchi, Switzerland) and the remaining film was hydrated with ultrapure water, sonicated, dialyzed and freeze-dried.

2.2.4. Au-MSS functionalization

The polymer functionalization of Au-MSS was performed using two different methodologies. In the first approach, TPGS-PEI co-polymer was used to modify the nanorods by promoting the electrostatic interaction between the negatively charged mesoporous silica surface and the positively charged amine groups on PEI. For that purpose, 5 mg of nanoparticles were resuspended with a TPGS-PEI co-polymer solution (5 mg/mL in ultrapure water). Then, this solution was vortexed for 1 min or 5 min, recovered by centrifugation (4,000g for 20 min at 25 ºC) and washed to remove the unreacted polymer, rendering the Au-MSS/TPGS-PEI (1 min) or (5 min) nanorods.

Alternatively, TPGS and PEI polymers were chemically linked to the Au-MSS surface by using a post-synthesis grafting methodology, as previously described in (158). Briefly, Au-MSS nanorods

(20 mg) were resuspended in 40 mL of EtOH (33 %, pH 4) and sonicated for 5 min. Then, TESPIC-TPGS and TESPIC-PEI polymers were added to the nanoparticles solution (TPGS/PEI ratio 1:1 or 3:1 in w/w). After 24 h, the final solution was centrifuged (8,000g, for 25 min at 25 ºC) and washed several times with ultrapure water to recover and remove the solvent from the Au-MSS/TPGS/PEI (1:1) or (3:1) nanorods.

2.2.5. Characterization of nanocarriers' physicochemical properties

2.2.5.1. Morphological characterization and size analysis

The morphology of both coated and uncoated Au-MSS rods was characterized by Transmission Electron Microscopy (TEM – Hitachi-HT7700, Japan). The nanoparticles samples were placed on formvar-coated copper grids and allowed to dry at room temperature. The images were acquired at an accelerating voltage of 100 kV. Afterward, nanoparticles total size, silica shell thickness, and gold core size were measured by using a specific software (Image J 2.0.0, NIH Image, USA).

2.2.5.2. Zeta potential analysis

The zeta potential measurement of coated and uncoated Au-MSS nanorods was performed by using a Zetasizer Nano ZS equipment (Malvern Instruments, Worcestershire, UK). In all the measurements, the nanoparticles were resuspended in ultrapure water, and the data was collected at 25 ºC in a disposable capillary cell.

2.2.5.3. Ultraviolet-visible spectroscopy analysis

The success of Au-MSS nanorods synthesis was evaluated through the acquisition of the particles' UV-vis spectra, using an UV-vis spectrophotometer (Thermo Scientific Evolution™ 201 Bio UV-vis Spectrophotometer, Thermo Fisher Scientific Inc., USA) at a 300 $nm.min^{-1}$ scanning rate, with a wavelength range from 200 to 1100 nm.

2.2.5.4. Fourier transform infrared spectroscopy analysis

Fourier transform infrared spectroscopy (FTIR) was used to evaluate the success of the Au-MSS nanorods purification process as well as their functionalization with the polymers. For that purpose, FTIR spectra of the nanoparticles were acquired on a Nicolet iS10 spectrometer, with a 4 cm^{-1} spectral resolution from 400 to 600 cm^{-1} (Thermo Scientific Inc., Massachusetts, USA). Moreover, in all the acquired data a baseline correction and atmospheric suppression were performed to avoid any possible interferences. Data analysis was executed in the OMNIC spectra software (Thermo Scientific).

2.2.5.5. Thermogravimetric analysis

The polymer content on the Au-MSS formulations was measured by performing the thermogravimetric analysis (TGA) of the samples. Briefly, uncoated or coated Au-MSS rods were heated up to 600 ºC, at a heating rate of 10 ºC/min under an inert atmosphere on a SDT Q600 equipment (TA Instruments, USA), and the particles' weight losses were recorded along time.

2.2.6. Drug loading

The Dox loading on coated or uncoated Au-MSS nanorods was performed through the impregnation of the particles in a Dox solution, as previously described by Moreira and co-workers (45). Briefly, the Au-MSS formulations were resuspended in 5.00 mL of methanol containing Dox (40 µg/mL), and sonicated for 15 min. Then, the solution was mixed under stirring for 48 h at room temperature. After that, the drug-loaded nanoparticles were recovered by centrifugation (18,000g for 20 min at 4 ºC) and freeze-dried. The supernatant was used to quantify the amount of drug loaded within nanoparticles.

The Dox content was calculated by measuring the supernatant absorbance at 485 nm, using a UV-vis Spectrophotometer (Thermo Scientific Evolution™ 201 Bio UV-vis Spectrophotometer, Thermo Fisher Scientific Inc., USA) and a calibration curve (ABS=16.715C-0.0006; r^2=0.9971). The encapsulation efficiency (EE) was calculated through equation (1):

$$EE\ (\%) = \frac{\text{Initial drug weight - Drug weight in the supernatant}}{\text{Initial drug weight}} \times 100 \qquad (1)$$

2.2.7. *In vitro* photothermal measurements

The evaluation of the *in vitro* photothermal capacity of coated and uncoated Au-MSS was performed as described in the literature (46). Thus, nanoparticles at a concentration of 100 µg/mL and a control group without particles were irradiated with a NIR laser (808 nm, 1.7 $W.cm^{-2}$). The temperature variation of the solution was measured at different time points (from 1 up to 10 min) by using a thermocouple sensor with an accuracy of 0.1 ºC.

2.2.8. Biocompatibility assays

2.2.8.1. Cell viability

The cell viability of coated and uncoated Au-MSS nanorods was evaluated through a resazurin-based assay (32). Briefly, HeLa cells were seeded into 96-well flat bottom culture plates at a density of 10,000 cells per well with 200 µL of DMEM-HG medium. During approximately 24 h, cells were cultured at 37 ºC in a humid atmosphere containing 5 % CO_2. Afterward, cells were cultured with different concentrations (25 to 200 µg/mL) of Au-MSS formulations. After 24 and 48 h of incubation, the medium was replaced and cells were incubated with medium containing resazurin (10 % v/v), at 37ºC and 5 % CO_2, for 4 h. The produced resorufin was quantified by

using a microwell plate reader (Spectramax Gemini XS, MolecularDevices LLC, USA) at an excitation/emission wavelength of λ_{ex} = 560 nm and λ_{em} = 590 nm. Cells cultured in the absence of nanoparticles were used as negative control (K^-), whereas cells incubated with EtOH (99.9 %) were used as positive control (K^+).

2.2.8.2 Evaluation of the Au-MSS effects on cells' migration ability

The wound closure assay was performed to evaluate the nanoparticles influence in the HeLa cells' migration ability (46). For that purpose, HeLa cells were seeded on 12-well flat bottom culture plates at a density of 50,000 cells per well, with 2 mL of medium. Cells were maintained in culture (at 37 ºC, in a humid atmosphere with 5 % CO_2), until reaching confluence. After this period, the medium was removed and a gap was made by using a micropipette tip. Then, cells were incubated with 100 µg/mL of the different Au-MSS formulations, during 24 and 48 h. A control group without particles was also monitored. Images were captured by using an Olympus CX41 inverted optical microscope equipped with an Olympus SP-500 UZ digital camera, and the cells' migration distance was measured using Image J software (Image J 2.0.0, NIH Image, USA).

2.2.9. Evaluation of the nanoparticle' cellular uptake

The Au-MSS formulations uptake by HeLa cells was characterized through confocal laser scanning microscopy (CLSM) following a protocol previously described by Gaspar and co-workers (159). For this purpose, 1 mg of each Au-MSS nanorods formulation was labeled with FITC.

For the analysis of the nanoparticles cellular uptake, 15,000 HeLa cells were seeded in µ-Slide 8 well Ibidi imaging plates and incubated for 48 h, at 37 ºC and 5 % CO_2. Afterward, cells were incubated with 200 µg/mL of Au-MSS formulations for 4 h. Subsequently, the seeded cells were washed with PBS, fixed with paraformaldehyde (4 % w/v) for 10 min and rinsed with PBS. For cell nucleus staining, cells were treated with Hoechst 33342®, whereas the cytoplasm of the cells was labeled with WGA-Alexa Flour 594®. The CLSM images were then acquired with a Zeiss LSM 710 Confocal microscope (Carl Zeiss SMT Inc., Germany) equipped with a Plan Apochromat 63x/1.4 Oil Differential Interference Contrast objective.

2.2.10. Statistical analysis

Data are presented as the mean ± standard deviation (s.d.). One-way analysis of variance (ANOVA) with the Student–Newman–Keuls post-test was used for multiple groups comparison. A p-value lower than 0.05 ($p<0.05$) was considered to be statistically significant. Statistical analysis was performed using GraphPad Prism v.6.0 software (Trial version, GraphPadSoftware, USA).

Chapter 3

Results and Discussion

3. Results and Discussion

3.1. Synthesis and characterization of TPGS-PEI, TESPIC-TPGS and TESPIC-PEI polymers

TPGS and PEI were selected for overcoming the Au-MSSs uncontrolled release profile, limited blood circulation and ultimately potentiate the therapeutic effect. TPGS, a water-soluble vitamin E derivative, has an amphiphilic nature and can act as solubilizer increasing the colloidal stability of these nanorods (160-162). In addition, TPGS can also act as an inhibitor of P-gp, a drug efflux pump overexpressed in cancer cells, and therefore improve the bioavailability of the chemotherapeutics (162, 163). On the other side, PEI is a cationic polymer routinely used to bind negatively charged cargos (164). In these nanorods, PEI will be attracted to the negatively charged mesoporous silica surface blocking the particle' pores and consequently the drug release. Moreover, the protonation of the amine groups, when in acidic environments, will also promote the nanoparticle escape from endocytic vesicles and lysosomes (164, 165).

Herein, TPGS and PEI were chemically modified to allow the posterior functionalization of the Au-MSS nanorods. Two different modifications were investigated (Figure 8), the TPGS linking to PEI through a CDI-mediated coupling reaction (TPGS-PEI co-polymer) (154, 155) and the individual modification of TPGS and PEI with TESPIC (TESPIC-TPGS and TESPIC-PEI silane derivatives) through a hydrogen-transfer nucleophilic addition reaction (156, 157). The TPGS-PEI, TESPIC-TPGS, and TESPIC-PEI modification was confirmed through FTIR analysis (Figure 9). The FTIR spectra of TPGS and TPGS-PEI co-polymer shows the characteristic peaks of TPGS at 1740 cm^{-1} and 1105 cm^{-1} corresponding to the vibration peak of C=O bond and C–O stretching vibration, respectively (166). Further, due to the inclusion of the PEI chain, it is also possible to observe the changes in the ratio between the peaks at 1146 cm^{-1} and 1052 cm^{-1}, which are attributed to the vibration of the PEI C-N bonds that also occur in the 1145 cm^{-1} region. The TESPIC-TPGS spectrum showed a distinctive absorption peak in the 1680-1640 cm^{-1} region assigned to the newly formed secondary amides. Moreover, the introduction of the silane moiety on the TPGS backbone also changed the spectrum in the 1110-1050 cm^{-1} region due to the absorption band of the Si-O-C bonds. Similar results were obtained for the TESPIC-PEI derivative, where it is possible to identify an absorption band on the 1110-1050 cm^{-1} region attributed to the Si-O-C bonds, indicating the successful PEI modification with the TESPIC.

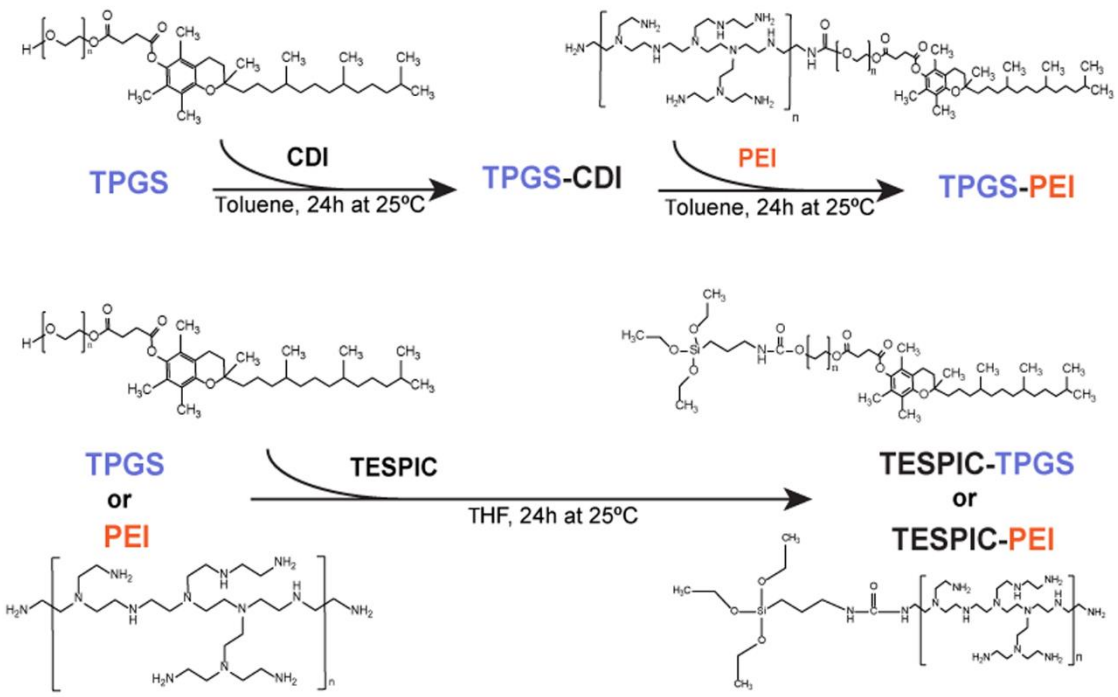

Figure 8 - Synthesis schematic of TPGS-PEI, TESPIC-TPGS, and TESPIC-PEI polymers.

3.2. Synthesis and characterization of Au-MSS nanorods

The Au-MSS rods were synthesized by using a seed-mediated methodology (46, 152, 153). The synthesis method involved three main steps: production by nucleation of small spherical gold particles that are then added to a growing solution to form the gold nanorods, and finally the production of the mesoporous silica shell coating using CTAB as a soft template to generate the pores. The successful synthesis of Au-MSS nanorods, with homogeneous distribution and organized in a single gold-core with a uniform silica shell, was confirmed via TEM images (please see Figure 10 A and B). The analysis of the TEM images show that the gold-core present a mean length and width of 43 ± 8 nm and 14 ± 3 nm, respectively, corresponding to an AR of 3.1 (Figure 11 A). Moreover, the Au-MSS nanorods presented a mean mesoporous silica shell thickness of ~22 nm resulting in particles with a total length and width of 84 ± 10 and 60 ± 4 nm, respectively (Figure 11 B). The obtained gold-core AR is compatible with the Au-MSS nanorods application in NIR-mediated PTT applications (76, 167). In fact, ARs between 3 and 4 have been reported has optimal to absorb the NIR light (167, 168). On the other side, the Au-MSS overall size still allows them to exploit the enhanced permeability and retention effect and therefore to accumulate passively in the tumor tissue (156).

The successful removal of the cytotoxic CTAB molecules from the Au-MSS was confirmed through FTIR (Figure 12). The Au-MSS nanorods spectrum does not contain the two characteristic bands of CTAB, between 2950 cm^{-1} and 2850 cm^{-1}, which correspond to the C-H vibration, and 1450-1500 cm^{-1}, that is attributed to CH_3-N^+ deformation (46). In addition, it is

possible to observe the mesoporous silica shell characteristic peaks in the 1100 to 750 cm^{-1} region, that correspond to Si-O-Si, Si-O and Si-OH vibrations (32). Therefore, this data indicates the successful purification of Au-MSS nanorods.

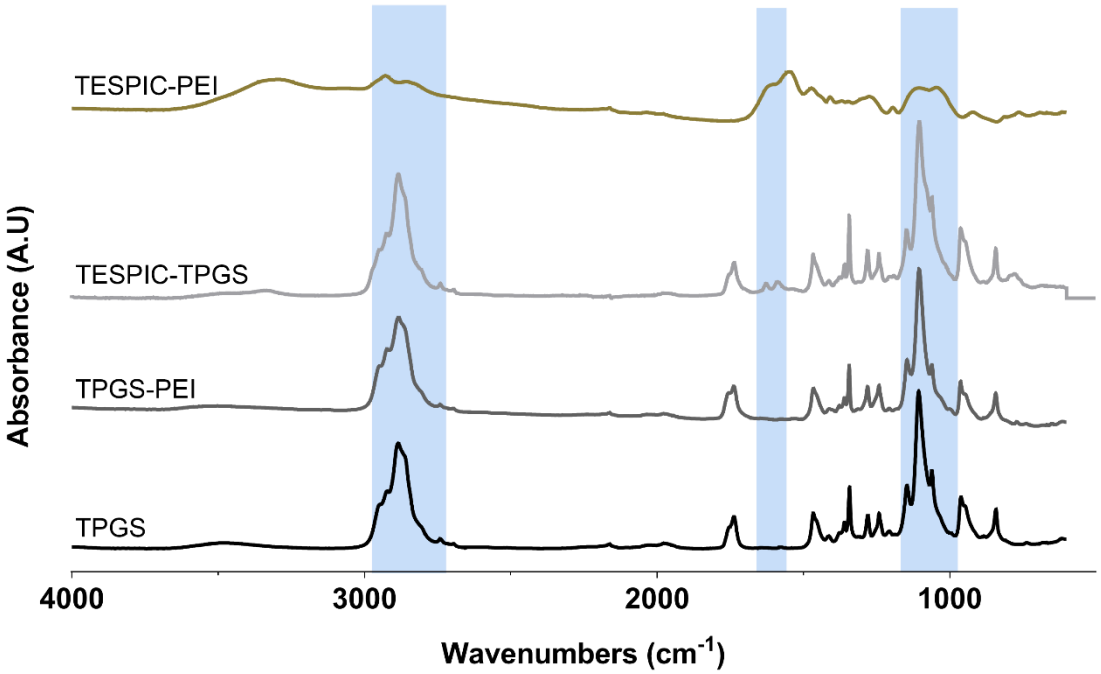

Figure 9 - FTIR spectra of TPGS, TPGS-PEI, TESPIC-TPGS and TESPIC-PEI polymers.

3.3. Synthesis and characterization of Au-MSS/TPGS-PEI and Au-MSS/TPGS/PEI nanoparticles

The Au-MSS nanorods were functionalized using two different approaches, through electrostatic interactions or by chemical linkage (Figure 10 C). The first approach is based on the establishment of the electrostatic interactions between the negatively charged surface of Au-MSS nanorods and positively charged amine groups on TPGS-PEI co-polymer. The chemical linkage was performed by promoting the grafting of the TESPIC-TPGS and TESPIC-PEI silane derivatives on the surface of the Au-MSS nanorods.

The Au-MSS nanorods surface functionalization was confirmed by measuring the zeta potential (Figure 11 C). The Au-MSS nanorods displayed a negative surface charge, -24.3 ± 3.7 mV, attributed to the presence of negatively charged silanol groups on the mesoporous silica surface. The Au-MSS/TPGS-PEI nanoparticles surface charge was dependent on the vortex time, the particles vortexed for 1 min presented a zeta potential of -5.1 ± 0.2 mV.

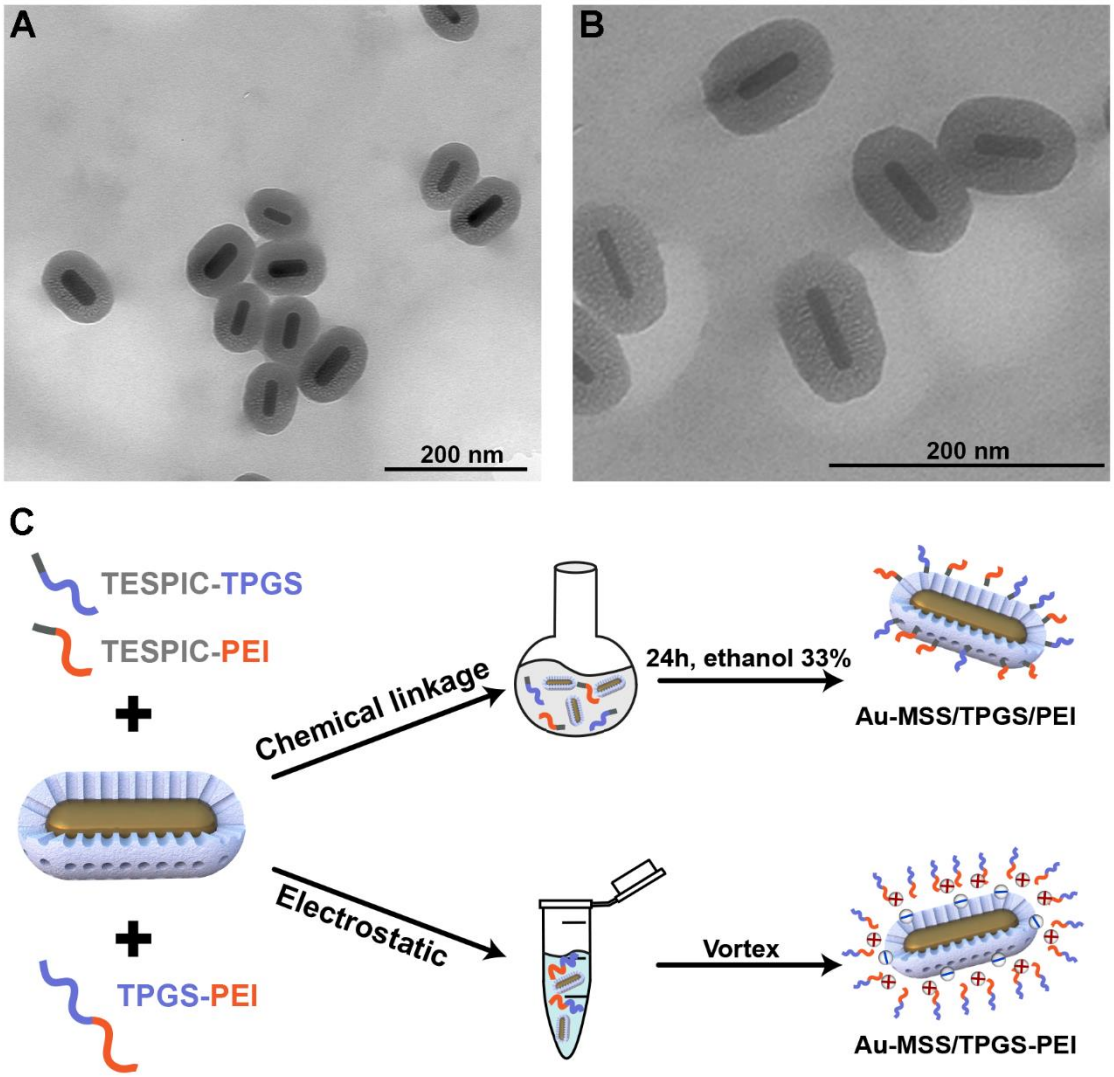

Figure 10 - Au-MSS synthesis and morphology analysis. (A) and (B) TEM images of Au-MSS nanorods at different magnifications. (C) Schematics synthesis of Au-MSS/TPGS-PEI and Au-MSS/TPGS/PEI nanoparticles.

Further, the increase in the vortex time to 5 min resulted in a more negative zeta potential, -16.9 ± 0.6 mV, which indicates a lower efficacy on functionalizing the particle surface. On the other side, the Au-MSS nanorods functionalized with TPGS/PEI (ratio 1:1) presented a zeta potential of +30.9 ± 5.7 mV, whereas the increase of the TPGS content (ratio 3:1) provoked a decrease on the surface charge to +6.8 ± 1.2 mV. Therefore, these results confirm the polymers binding to the Au-MSS surface, since the changes observed on the surface charge are explained by the positively charged amine groups present on the PEI. Additionally, in the Au-MSS/TPGS/PEI (3:1), the reduction on the surface charge may also indicate a reduction in the amount of PEI chains grafted on the particle surface, when compared with the Au-MSS/TPGS/PEI (1:1). As described in the literature, the nanoparticles pharmacokinetic profile, blood circulation time and biocompatibility are highly influenced by their surface charge (169, 170). In fact, a neutral surface charge (± 10 mV) is until now considered the ideal for nanoparticles circulation, whereas slightly positive particles often present a higher

internalization by the cells (171, 172). Taking this into account, only the Au-MSS/TPGS-PEI (1 min), Au-MSS/TPGS/PEI (1:1) and Au-MSS/TPGS/PEI (3:1) formulations were selected for the subsequent studies.

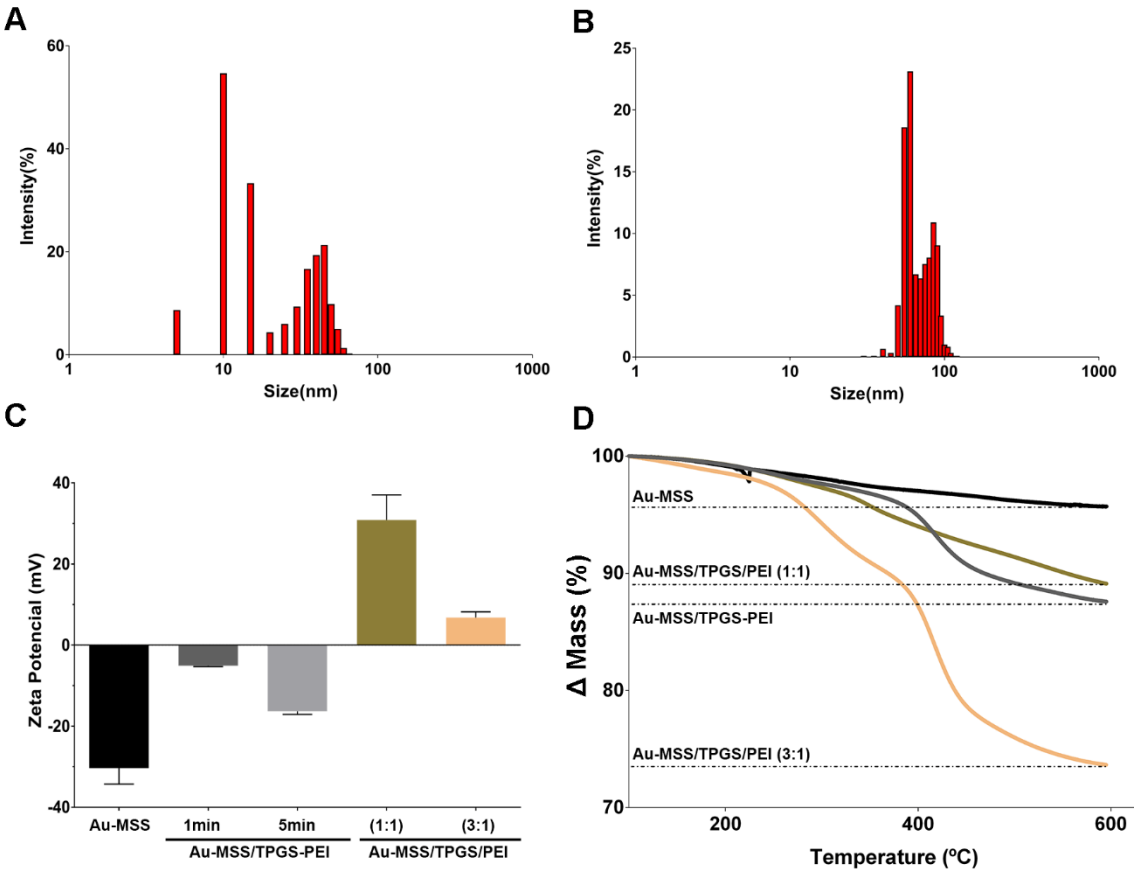

Figure 11 - Physicochemical characterization of Au-MSS formulations. A) Gold nanorods size distribution (length and width included), n=300. (B) Au-MSS size distribution (length and width included), n=300. (C) Surface charge analysis of Au-MSS, Au-MSS/TPGS-PEI and Au-MSS/TPGS/PEI formulations, n=3. (D) TGA analysis of Au-MSS, Au-MSS/TPGS/PEI (1:1), Au-MSS/TPGS/PEI (3:1) and Au-MSS/TPGS-PEI (1 min).

The Au-MSS nanorods modification with the polymers was further confirmed by FTIR (Figure 12). The Au-MSS/TPGS-PEI (1 min) spectra showed the characteristic peaks of the silica shell on the 1100 to 750 cm^{-1} region and additionally, the presence of peaks at 2900 cm^{-1} and 1700 cm^{-1} regions assigned to the TPGS and PEI, respectively. Similar results were observed on the Au-MSS/TPGS/PEI (1:1) and Au-MSS/TPGS/PEI (3:1) formulations. Moreover, the successful grafting of the silane-modified polymers on the surface of nanorods was also confirmed by the increase of the ratio between the Si-O-Si peak at 1045 cm^{-1} and Si-OH peak at 950 cm^{-1}. Such is justified by the reduction of the nanoparticle Si-OH surface groups due to the TPGS/TESPIC and PEI/TESPIC condensation on the Au-MSS surface.

Additionally, the Au-MSS nanorods polymer content was determined by performing a thermogravimetric analysis (Figure 11 D). The weight losses observed for Au-MSS nanorods were

minimal and can be attributed to the evaporation of water in the interior of the mesopores and to the loss of the functional hydroxyl groups (Si-OH) on the surface of the particles (173, 174). On the other side, the recorded weight losses were superior for the Au-MSS/TPGS-PEI, Au-MSS/TPGS/PEI (1:1) and Au-MSS/TPGS/PEI (3:1), which is attributed to the polymers pyrolysis and corroborates the successful functionalization of the nanorods by both methodologies. The calculated polymer content for Au-MSS/TPGS-PEI, Au-MSS/TPGS/PEI (1:1) and Au-MSS/TPGS/PEI (3:1) was 12 %, 10 % and 25 %, respectively. The higher polymer content obtained with the increase of the TPGS/PEI ratio on Au-MSS/TPGS/PEI (1:1) and Au-MSS/TPGS/PEI (3:1) nanorods may be justified by a reduction of the electrostatic repulsion between the PEI chains, thus favoring the polymer grafting on the particles surface.

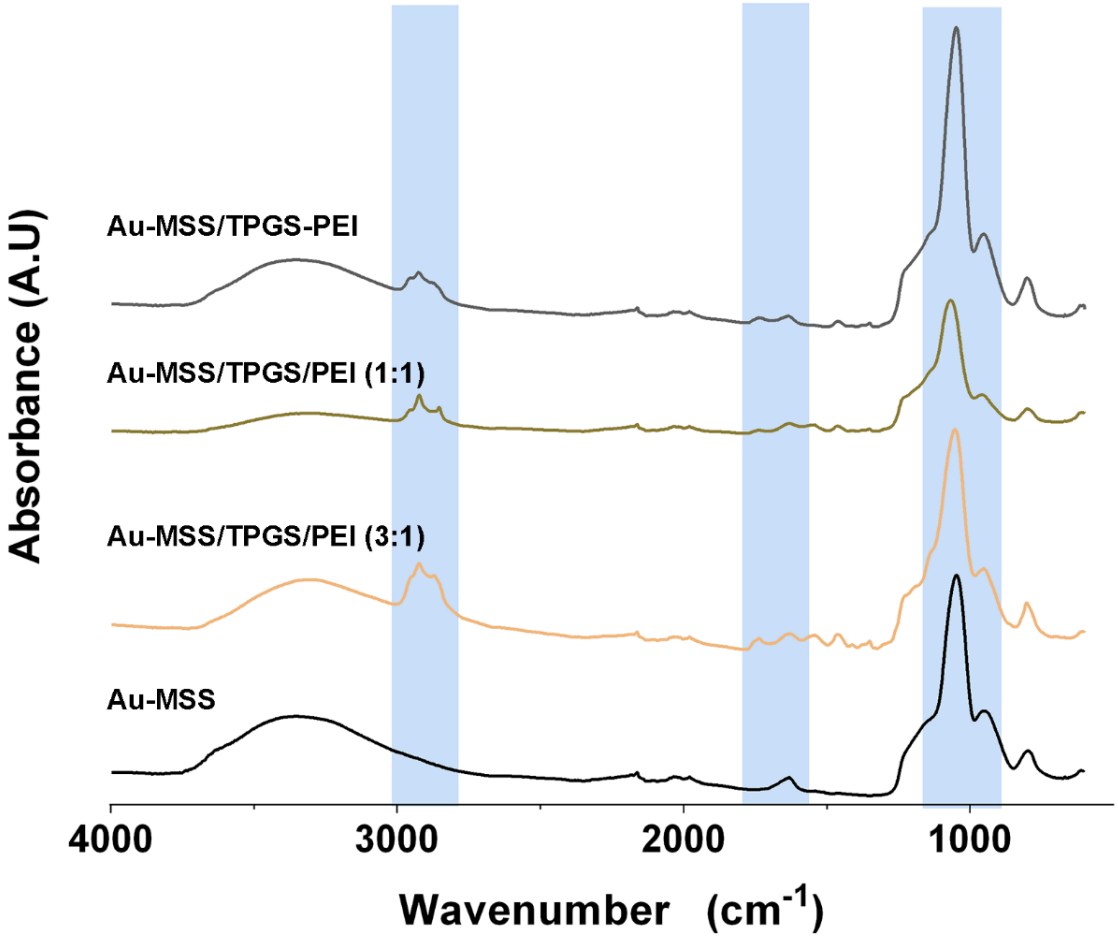

Figure 12 - FTIR spectra of Au-MSS, Au-MSS/TPGS/PEI (3:1), Au-MSS/TPGS/PEI (1:1) and Au-MSS/TPGS-PEI (1 min).

3.4. Drug loading capacity of Au-MSS derivatives

The Au-MSS capacity to encapsulate chemotherapeutic drugs was characterized by measuring the encapsulation efficiency of Dox (Figure 13). The Dox loading was promoted by resuspending the Au-MSS nanoparticles (*i.e.* Au-MSS and Au-MSS/TPGS/PEI) in Dox solution for 48 h. For the Au-MSS/TPGS-PEI nanorods, the loading was performed before the Au-MSS functionalization with the TPGS-PEI co-polymer (Figure 13 A). The obtained results showed that all the Au-MSS

formulations are able to encapsulate Dox (Figure 13 B). Both Au-MSS and Au-MSS/TPGS-PEI nanorods presented an encapsulation efficiency superior to 50 % (*i.e.* 10 µg of Dox per Au-MSS mg). This data indicates that no significant drug losses occur during the Au-MSS functionalization with the TPGS-PEI co-polymer. On the other side, the encapsulation efficiency decreased for around 20 % on Au-MSS/TPGS/PEI (1:1) and 30 % for on Au-MSS/TPGS/PEI (3:1) formulations. This decrease in the encapsulation efficiency can be attributed to the blockage of the Au-MSS mesopores by the TPGS and PEI polymers or even to a repulsion phenomenon between the positively charged PEI chains and Dox molecules.

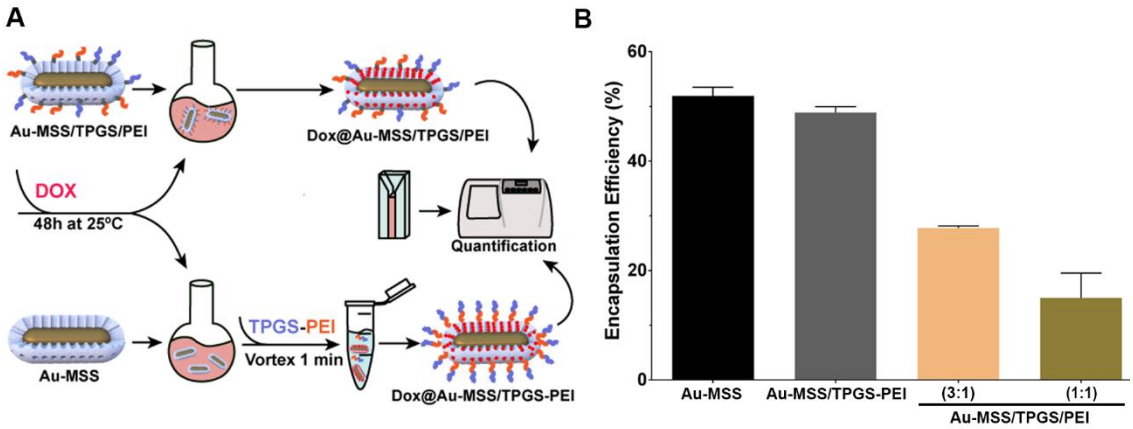

Figure 13 - Characterization of Dox encapsulation efficiency. (A) Schematics of the two methodologies of drug loading for Au-MSS/TPGS/PEI and Au-MSS/TPGS-PEI formulations. (B) Dox encapsulation efficiency on Au-MSS, Au-MSS/TPGS-PEI (1 min), Au-MSS/TPGS/PEI (3:1) and (1:1) nanorods. Data are presented as mean ± s.d., *p<0.05, n= 3.

3.5. *In vitro* evaluation of the photothermal capacity of nanoparticles

The potential application of Au-MSS derivatives on PTT was firstly assessed by acquiring their UV-vis absorption spectrum (Figure 14 B). The Au-MSS nanorods present two characteristics absorption peaks at 515 nm and 750 nm (*i.e.* NIR region) that correspond to the transverse and longitudinal resonances, respectively. Moreover, the functionalization with TPGS-PEI or TESPIC-TPGS and TESPIC-PEI did not induce any significant changes in the absorption capacity of the nanorods. This strong absorption in the 700-900 nm range supports the Au-MSS derivatives application in PTT. Further, reduced off-target interactions are expected since the biologic constituents present a low absorption to this radiation (175, 176).

After confirming the NIR absorption of Au-MSS derivatives, their capacity to convert optical energy into heat was investigated by measuring the temperature changes induced by the nanoparticles upon NIR laser irradiation (Figure 14 A). In Figure 14 C and D, it is possible to observe that all the Au-MSS derivatives could induce an increase in the temperature when irradiated with the NIR laser for up to 10 min. In addition, the polymers inclusion did not affect

the obtained results, being all the formulations capable to produce a temperature variation of about 40 ºC. This increase in the temperature can provoke the denaturation of proteins, disruption of cells' membrane, dysfunction of metabolic functions and consequently lead to the cancer cells' death. Further, it is worth to notice that even when this assay was performed in complex media (*i.e.* DMEM-HG medium supplemented with 10 % FBS), the performance of the Au-MSS/TPGS-PEI, Au-MSS/TPGS/PEI (1:1) and Au-MSS/TPGS/PEI (3:1) nanorods was not affected (Figure 14 C and D). Such findings indicate a good particle stability since their aggregation can induce changes in the absorption spectra of the nanorods and consequently affect their PTT capacity (177, 178).

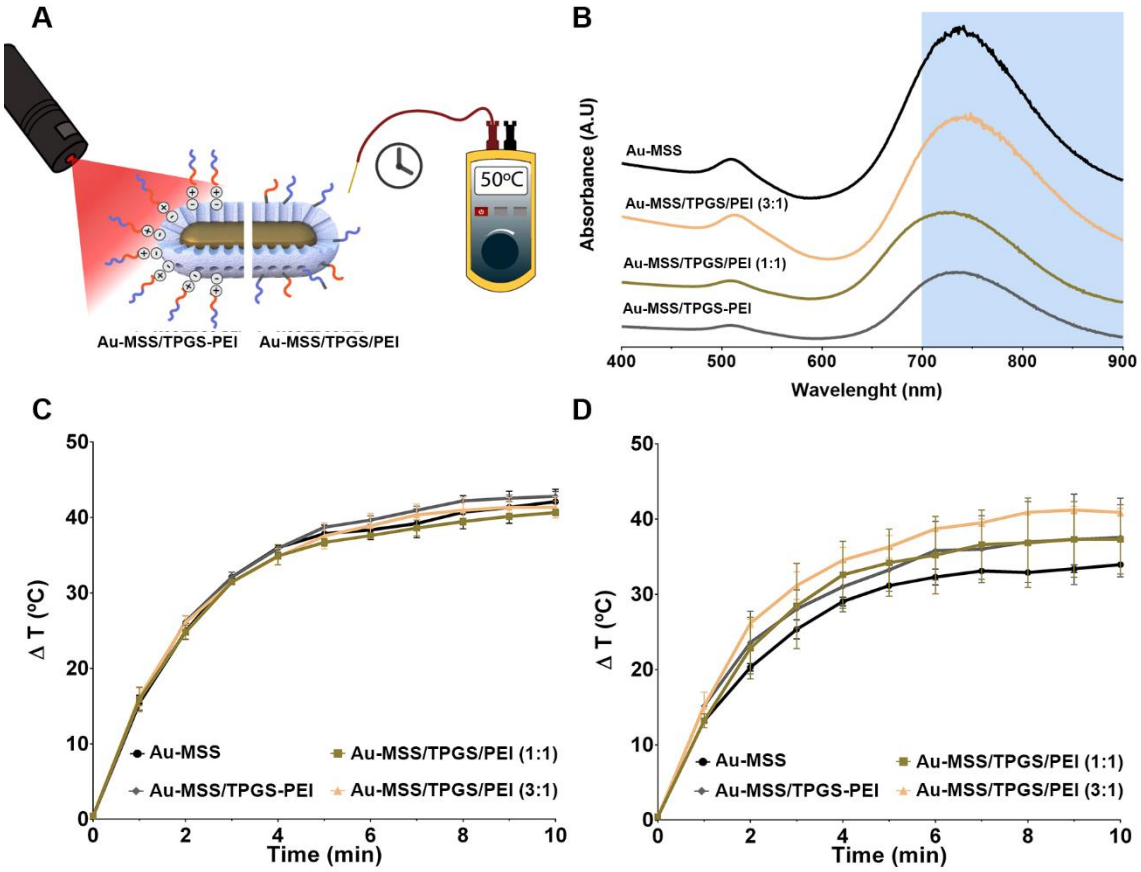

Figure 14 - Characterization of the PTT capacity of Au-MSS nanorods and its derivatives. (A) Schematics of the evaluation of Au-MSS formulations *in vitro* PTT capacity. (B) UV-vis spectra of Au-MSS and derivatives nanorods. (C) Temperature variation curve of Au-MSS derivatives in complex media (DMEM-HG), NIR laser (808 nm, 1.7 W.cm^{-2}) irradiation for 10 min. (D) Temperature variation curve of Au-MSS and Au-MSS derivatives in ultrapure water, NIR laser (808 nm, 1.7 W.cm^{-2}) irradiation for 10 min. Data are presented as mean ± s.d., *p<0.05, n= 3.

3.6. Nanoparticles biocompatibility

3.6.1. Cell viability

The cell viability of non-coated Au-MSS nanorods and its coated derivatives was evaluated on HeLa cancer cells. It is important to notice that a reduction of cell viability by more than 30 %

is considered a cytotoxic effect. The different nanoparticle formulations were incubated for 24 and 48 h with HeLa cells, at concentrations ranging from 25 to 200 µg/mL (Figure 15).

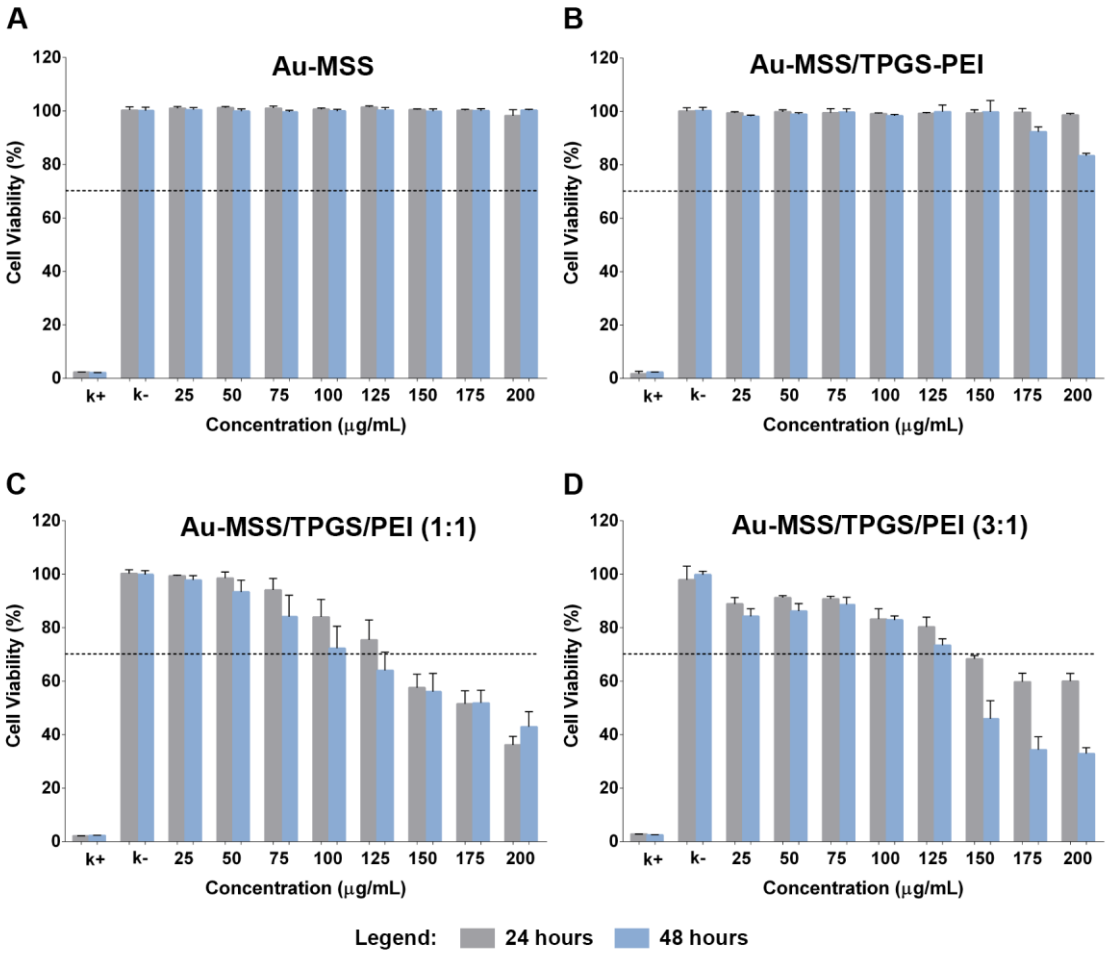

Figure 15 - Evaluation of Au-MSS derivatives biocompatibility in HeLa cells at 24 and 48 h. (A) Biocompatibility analysis for Au-MSS, (B) Au-MSS/TPGS-PEI (1 min), (C) Au-MSS/TPGS/PEI (1:1) and (D) Au-MSS/TPGS/PEI (3:1) nanorods. Positive control (K^+): cells treated with EtOH; negative control (K^-): cells without nanoparticles incubation. Data are presented as mean ± s.d., * $p<0.05$, n = 5.

The Au-MSS nanorods did not reveal any toxicity towards Hela cells, being registered cell viabilities superior to 70 %, even at a concentration of 200 µg/mL (Figure 15 A). These results are in agreement with different reports available in the literature, where Au-MSS with a rod-like, spherical or other shape were biocompatible with human dermal fibroblasts, HepG2 and HeLa cells (46, 135). Similar results were observed for Au-MSS/TPGS-PEI nanorods. The HeLa cells incubated with Au-MSS/TPGS-PEI (1 min) nanorods at concentrations up to 200 µg/mL also presented cell viabilities superior to 70 % after 48 h of incubation (Figure 15 B). On the other side, the Au-MSS/TPGS/PEI (1:1) nanoparticles induced a dose-dependent variation on the cell viability of the HeLa cells (Figure 15 C). The cells presented a viability of ~80 % at a concentration of 100 µg/mL and continued to decrease to almost 20 % with the increase of the

nanoparticles concentration up to 200 µg/mL. These results can be explained by the high positive charge density within the PEI chains that can lead to the destabilization of the cell membrane and cellular necrosis. So, in this way, the Au-MSS/TPGS/PEI (3:1) nanoparticles, which present a lower PEI content, displayed a superior cell biocompatibility (Figure 15 D). The results revealed that the HeLa cells treated with Au-MSS/TPGS/PEI (3:1) nanorods up to 125 µg/mL presented cell viabilities superior to 70 %.

3.6.2. Evaluation of the Au-MSS effect on cells' migration ability

To further characterize the biocompatibility of the Au-MSS formulations, the nanoparticles effect on the HeLa cells' migration ability was also evaluated (please see the Figure 16 and Appendix 1). The obtained results reveal that both Au-MSS and Au-MSS/TPGS-PEI nanorods did not induce any negative effect on HeLa cells motility. In Figure 16 A and B, it is possible to observe that the Control, Au-MSS, and Au-MSS/TPGS-PEI formulations presented almost 45 % decrease on the gap width in only 48 h of incubation. These data are in accordance with the previous works were Au-MSS nanorods were reported as being biocompatible even when high concentrations were used (46). Further, this result also supports the good biocompatibility demonstrated by Au-MSS/TPGS-PEI nanorods in the cell viability studies.

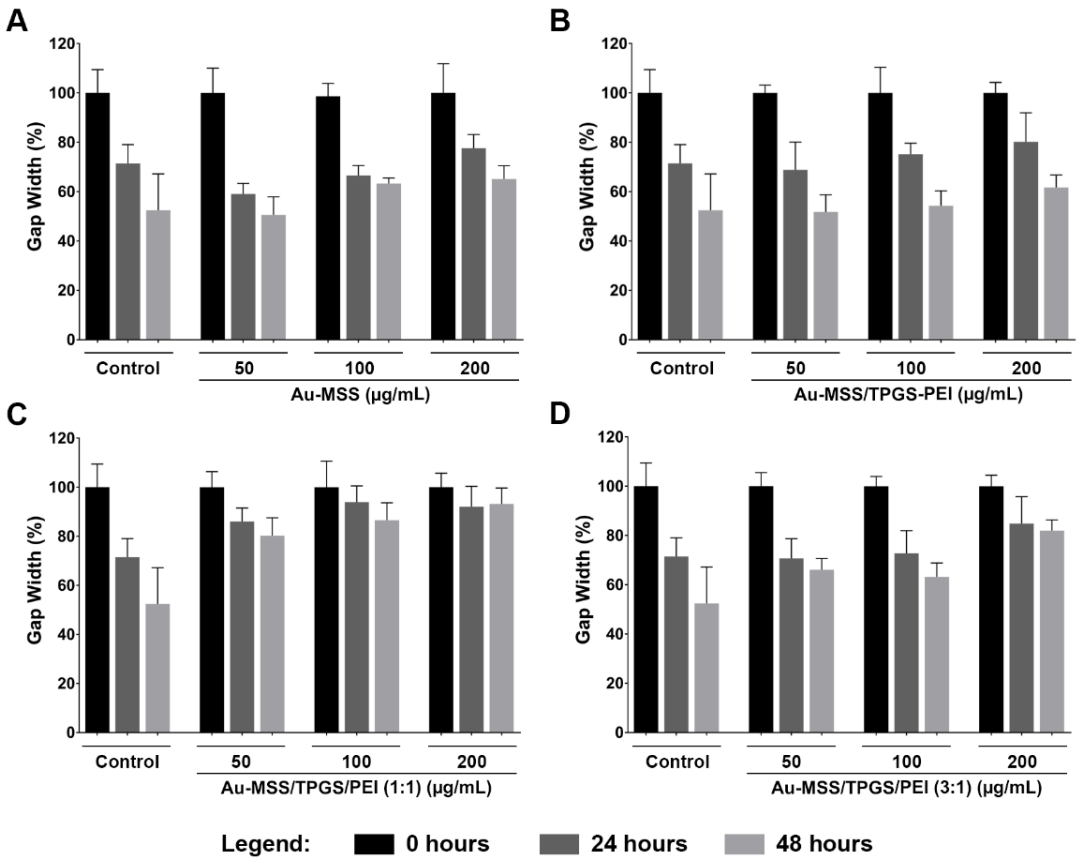

Figure 16 - Evaluation of Au-MSS derivatives effect on the migration ability of HeLa cells at 24 and 48 h. (A) Gap Width analysis for Au-MSS, (B) Au-MSS/TPGS-PEI (1 min), (C) Au-MSS/TPGS/PEI (1:1) and (D) Au-MSS/TPGS/PEI (3:1) nanorods. Control: cells without nanoparticles incubation. Data are presented as mean ± s.d., * $p<0.05$, n = 3.

In the other side, the cells treated with Au-MSS/TPGS/PEI nanorods presented a higher gap width (Figure 16 C and D). The Au-MSS/TPGS/PEI (3:1) did not affect the HeLa cells motility when the concentration was inferior or equal to 100 µg/mL, whereas the cells incubated with Au-MSS/TPGS/PEI (1:1) showed an impaired motility even at the lowest tested concentration, *i.e.* 50 µg/mL. These results confirm the data obtained during the cell viability analysis, where the positive charge of PEI impacts the particles biocompatibility by promoting the destabilization of the cell membrane and cellular necrosis. Further, similarly to the previously observed, the decrease of the PEI content on the Au-MSS/TPGS/PEI (3:1) formulation also led to a better biological performance.

3.7. Evaluation of the nanoparticle' cellular uptake

After assessing the biocompatibility of Au-MSS formulations, the nanoparticles cellular uptake was evaluated by using confocal microscopy. The nanoparticles' cellular uptake is one of the most important barriers that drug delivery systems have to overcome when applied in cancer therapy. In this study, the nanoparticles tracking was achieved by labeling Au-MSS nanorods with FTIC. In Figure 17, it is possible to observe the internalization of all Au-MSS formulations. These data are in agreement with previous studies where it was demonstrated the nanorods capacity to transpose the cell membrane, even with a superior efficiency than the spherical counterparts (46, 148, 179). Additionally, the CLSM images (Figure 17) also indicate that the functionalization of Au-MSS nanorods with TPGS and PEI improves the nanoparticles' uptake. Despite the differences in the synthesis methodology, the Au-MSS/TPGS-PEI and Au-MSS/TPGS/PEI (3:1) treated groups do not show any significative difference on the Au-MSS cellular internalization, which may be attributed to their neutral surface charge (*i.e.* -5.1 and +6.8, respectively) Surprisingly, the Au-MSS/TPGS/PEI (1:1) formulation, which presents a highly positive surface charge, appear to have a lower internalization on HeLa cells. Such result may be explained by the higher PEI content that has been associated with the disruption of the cell membrane and consequent lower biocompatibility.

Altogether, this data indicates that the synthesis methodology used for functionalizing the Au-MSS nanorods, electrostatic interaction or chemical linkage, may not influence the nanoparticles cellular uptake. Further, the Au-MSS/TPGS-PEI and Au-MSS/TPGS/PEI (3:1) formulations were successfully internalized by HeLa cells, which will allow the drug release in cell cytoplasm thus avoiding the premature drug degradation and increasing the therapeutic potential.

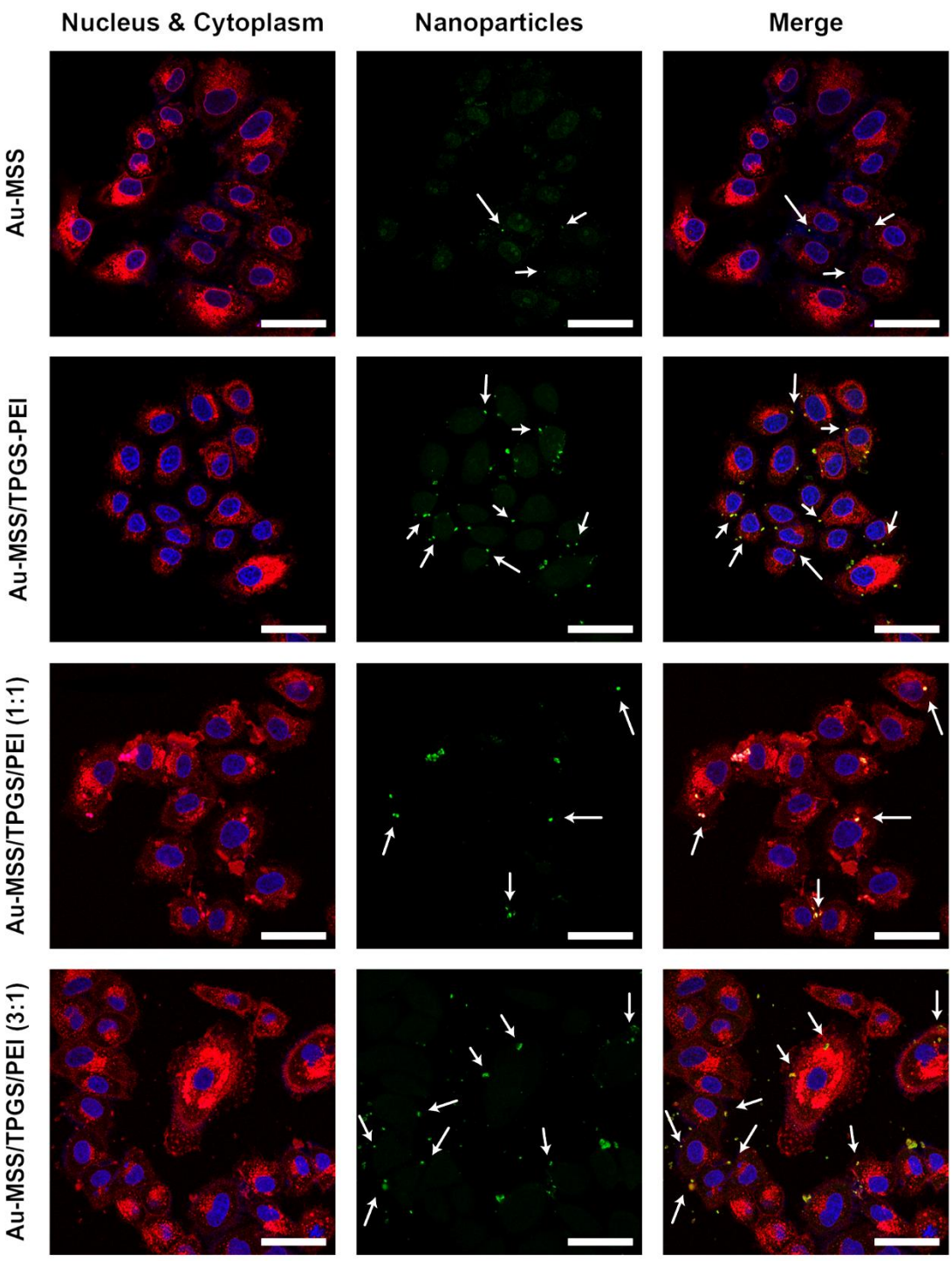

Figure 17 - Representative confocal microscopy images of Au-MSS formulations uptake by HeLa cells. The white arrows are pointing to the internalized nanoparticles. The scale bar corresponds to 50 µm. Blue channel: Hoechst 33342® stained cell nucleus; red channel: WGA-Alexa Fluor 594® stained cell cytoplasm; green channel: FITC labeled nanoparticles.

Chapter 4

Conclusion and Future Perspectives

4. Conclusion and Future Perspectives

Nowadays there is a demand for novel and more effective anti-cancer therapeutics. The recent breakthroughs in the nanotechnology field started a new era of anti-cancer medicines. Among the plethora of nanoparticles that have been developed so far, the Au-MSS nanoparticles display advantageous physicochemical and biological properties that make them promising nanoplatforms for cancer therapy.

The Au-MSS nanorods are multifunctional nanomaterials that can act simultaneously as drug delivery, photothermal and bioimaging agents. However, it is essential to improve nanoparticles' blood circulation time and drug release profile, when biological applications are intended. For that purpose, in this study, two different methodologies were explored and optimized to functionalize Au-MSS nanorods with TPGS and PEI in order to increase the colloidal stability of these nanorods and avoid the drug leakage. Polymer coated Au-MSS nanorods were produced by promoting the electrostatic adsorption of TPGS-PEI co-polymer or the chemical grafting of each polymer individually on the particle surface. The obtained results demonstrate that the Au-MSS nanorods functionalization did not impact on the nanorods overall size and on their PTT potential. Further, the synthesis methodology and polymer ratio influenced the nanorods surface charge as well as their capacity to encapsulate Dox. The *in vitro* assays showed that the Au-MSS and Au-MSS/TPGS-PEI were biocompatible at concentrations up to 200 μg/mL, whereas these values were slightly lower for Au-MSS/TPGS/PEI (1:1) and (3:1), 100 and 125 μg/mL respectively. Moreover, the Au-MSS/TPGS-PEI and Au-MSS/TPGS/PEI (3:1) formulations were successfully internalized by HeLa cells. Overall, the attained data confirm the successful modification of Au-MSS nanorods with TPGS and PEI polymers. Additionally, the Au-MSS/TPGS-PEI (1 min) formulation showed the most promising physicochemical and biological properties, followed by Au-MSS/TPGS/PEI (3:1) nanorods, for being applied in cancer chemotherapy, PTT, and imaging.

In the near future, the PEI capacity to imprint a controlled drug release to Au-MSS nanorods will be characterized at both physiological and acidic pH (TME). Moreover, the anti-cancer potential of Au-MSS formulations and the possible synergic effect resulting from the chemotherapy and PTT combination will be characterized both with 2D and 3D cell culture models. Then, the most promising formulation will proceed to *in vivo assays* to explore the biopolymers potential to improve the nanoparticles biodistribution as well as to characterize the Au-MSS biosafety and anti-tumoral effect. Accordingly, to the obtained data, the polymer content or TPGS/PEI ratio on the nanoparticles surface can be further optimized. Additionally, targeting moieties can be attached to the particle surface for increasing the Au-MSS selectivity to cancer cells, towards an improved therapeutic outcome and ultimately enhancing the patients' life expectancy and well-being.

Chapter 5

References

5. References

1. Torre LA, Bray F, Siegel RL, Ferlay J, Lortet-Tieulent J, Jemal A. Global Cancer Statistics, 2012. CA Cancer J Clin. 2015;65(2):87-108.
2. Siegel RL, Miller KD, Jemal A. Cancer Statistics, 2018. CA Cancer J Clin. 2018;68(1):7-30.
3. Miranda N, Gonçalves MB, Andrade C, Santos G. Programa Nacional para as Doenças Oncológicas. Direção-Geral da Saúde 2017.
4. Vineis P, Wild CP. Global cancer patterns: causes and prevention. Lancet. 2014;383(9916):549-57.
5. Quail DF, Joyce JA. Microenvironmental regulation of tumor progression and metastasis. Nat Med. 2013;19(11):1423-37.
6. Floor SL, Dumont JE, Maenhaut C, Raspe E. Hallmarks of cancer: of all cancer cells, all the time? Trends Mol Med. 2012;18(9):509-15.
7. Hanahan D, Weinberg RA. The hallmarks of cancer. Cell. 2000;100(1):57-70.
8. Pietras K, Ostman A. Hallmarks of cancer: Interactions with the tumor stroma. Exp Cell Res. 2010;316(8):1324-31.
9. Bussard KM, Mutkus L, Stumpf K, Gomez-Manzano C, Marini FC. Tumor-associated stromal cells as key contributors to the tumor microenvironment. Breast Cancer Res. 2016;18.
10. Klemm F, Joyce JA. Microenvironmental regulation of therapeutic response in cancer. Trends Cell Biol. 2015;25(4):198-213.
11. Xu X, Farach-Carson MC, Jia XQ. Three-dimensional in vitro tumor models for cancer research and drug evaluation. Biotechnol Adv. 2014;32(7):1256-68.
12. Vannucci L. Stroma as an Active Player in the Development of the Tumor Microenvironment. Cancer Microenviron. 2015;8(3):159-66.
13. Hanahan D, Weinberg RA. Hallmarks of Cancer: The Next Generation. Cell. 2011;144(5):646-74.
14. Giampazolias E, Tait SWG. Mitochondria and the hallmarks of cancer. Febs J. 2016;283(5):803-14.
15. Muller PAJ, Vousden KH. Mutant p53 in Cancer: New Functions and Therapeutic Opportunities. Cancer Cell. 2014;25(3):304-17.
16. Liu TT, Yuan XT, Xu DW. Cancer-Specific Telomerase Reverse Transcriptase (TERT) Promoter Mutations: Biological and Clinical Implications. Genes. 2016;7(7).
17. Yadav L, Puri N, Rastogi V, Satpute P, Sharma V. Tumour Angiogenesis and Angiogenic Inhibitors: A Review. J Clin Diagn Res. 2015;9(6):Xe1-Xe5.
18. Goel HL, Mercurio AM. VEGF targets the tumour cell. Nat Rev Cancer. 2013;13(12):871-82.

19. Ernsting MJ, Murakami M, Roy A, Li SD. Factors controlling the pharmacokinetics, biodistribution and intratumoral penetration of nanoparticles. J Controlled Release. 2013;172(3):782-94.
20. Canel M, Serrels A, Frame MC, Brunton VG. E-cadherin–integrin crosstalk in cancer invasion and metastasis. J Cell Sci. 2013;126(2):393-401.
21. DeSantis CE, Lin CC, Mariotto AB, Siegel RL, Stein KD, Kramer JL, et al. Cancer treatment and survivorship statistics, 2014. CA Cancer J Clin. 2014;64(4):252-71.
22. Runowicz CD, Leach CR, Henry NL, Henry KS, Mackey HT, Cowens-Alvarado RL, et al. American cancer society/American society of clinical oncology breast cancer survivorship care guideline. CA Cancer J Clin. 2016;66(1):43-73.
23. Hu Q, Sun W, Wang C, Gu Z. Recent advances of cocktail chemotherapy by combination drug delivery systems. Adv Drug Delivery Rev. 2016;98:19-34.
24. Holohan C, Van Schaeybroeck S, Longley DB, Johnston PG. Cancer drug resistance: an evolving paradigm. Nat Rev Cancer. 2013;13(10):714.
25. Brown R, Links M. Clinical relevance of the molecular mechanisms of resistance to anti-cancer drugs. Expert Rev Mol Med. 1999;1(15):1-21.
26. Rebucci M, Michiels C. Molecular aspects of cancer cell resistance to chemotherapy. Biochem Pharmacol. 2013;85(9):1219-26.
27. Al-Lazikani B, Banerji U, Workman P. Combinatorial drug therapy for cancer in the post-genomic era. Nat Biotechnol. 2012;30(7):679.
28. Sharom FJ. Complex interplay between the P-glycoprotein multidrug efflux pump and the membrane: its role in modulating protein function. Front Oncol. 2014;4:41.
29. Dong X, Mumper RJ. Nanomedicinal strategies to treat multidrug-resistant tumors: current progress. Nanomedicine. 2010;5(4):597-615.
30. Parhi P, Mohanty C, Sahoo SK. Nanotechnology-based combinational drug delivery: an emerging approach for cancer therapy. Drug discovery today. 2012;17(17-18):1044-52.
31. Balasubramanian V, Liu Z, Hirvonen J, Santos HA. Bridging the knowledge of different worlds to understand the big picture of cancer nanomedicines. Adv Healthcare Mater. 2018;7(1):1700432.
32. Moreira AF, Gaspar VM, Costa EC, de Melo-Diogo D, Machado P, Paquete CM, et al. Preparation of end-capped pH-sensitive mesoporous silica nanocarriers for on-demand drug delivery. Eur J Pharm Biopharm. 2014;88(3):1012-25.
33. Cai Z, Yook S, Lu Y, Bergstrom D, Winnik MA, Pignol J-P, et al. Local Radiation Treatment of HER2-Positive Breast Cancer Using Trastuzumab-Modified Gold Nanoparticles Labeled with 177 Lu. Pharm Res. 2017;34(3):579-90.
34. Mancini S, Minniti S, Gregori M, Sancini G, Cagnotto A, Couraud P-O, et al. The hunt for brain Aß oligomers by peripherally circulating multi-functional nanoparticles: Potential therapeutic approach for Alzheimer disease. Nanomedicine: (NBM). 2016;12(1):43-52.

35. Ruff J, Hüwel S, Kogan MJ, Simon U, Galla H-J. The effects of gold nanoparticles functionalized with ß-amyloid specific peptides on an in vitro model of blood–brain barrier. Nanomedicine: (NBM). 2017;13(5):1645-52.
36. Yoo J, Lee E, Kim HY, Youn D-h, Jung J, Kim H, et al. Electromagnetized gold nanoparticles mediate direct lineage reprogramming into induced dopamine neurons in vivo for Parkinson's disease therapy. Nat Nanotechnol. 2017;12(10):1006.
37. Hernando S, Herran E, Figueiro-Silva J, Pedraz JL, Igartua M, Carro E, et al. Intranasal Administration of TAT-Conjugated Lipid Nanocarriers Loading GDNF for Parkinson's Disease. Mol Neurobiol. 2017:1-11.
38. Moreira AF, Dias DR, Correia IJ. Stimuli-responsive mesoporous silica nanoparticles for cancer therapy: A review. Microporous Mesoporous Mater. 2016;236:141-57.
39. Xu X, Ho W, Zhang X, Bertrand N, Farokhzad O. Cancer nanomedicine: from targeted delivery to combination therapy. Trends Mol Med. 2015;21(4):223-32.
40. Blanco E, Shen H, Ferrari M. Principles of nanoparticle design for overcoming biological barriers to drug delivery. Nat Biotechnol. 2015;33(9):941.
41. Albanese A, Tang PS, Chan WC. The effect of nanoparticle size, shape, and surface chemistry on biological systems. Annu Rev Biomed Eng. 2012;14:1-16.
42. Wicki A, Witzigmann D, Balasubramanian V, Huwyler J. Nanomedicine in cancer therapy: challenges, opportunities, and clinical applications. J Controlled Release. 2015;200:138-57.
43. Dixit S, Novak T, Miller K, Zhu Y, Kenney ME, Broome A-M. Transferrin receptor-targeted theranostic gold nanoparticles for photosensitizer delivery in brain tumors. Nanoscale. 2015;7(5):1782-90.
44. Gaspar VM, Costa EC, Queiroz JA, Pichon C, Sousa F, Correia IJ. Folate-targeted multifunctional amino acid-chitosan nanoparticles for improved cancer therapy. Pharm Res. 2015;32(2):562-77.
45. Moreira AF, Dias DR, Costa EC, Correia IJ. Thermo-and pH-responsive nano-in-micro particles for combinatorial drug delivery to cancer cells. Eur J Pharm Sci. 2017;104:42-51.
46. Dias DR, Moreira AF, Correia IJ. The effect of the shape of gold core–mesoporous silica shell nanoparticles on the cellular behavior and tumor spheroid penetration. J Mater Chem B. 2016;4(47):7630-40.
47. La-Beck NM, Gabizon AA. Nanoparticle interactions with the immune system: Clinical implications for liposome-based cancer chemotherapy. Front Immunol. 2017;8:416.
48. Yildirimer L, Thanh NT, Loizidou M, Seifalian AM. Toxicology and clinical potential of nanoparticles. Nano today. 2011;6(6):585-607.
49. Zhang L, Gu F, Chan J, Wang A, Langer R, Farokhzad O. Nanoparticles in medicine: therapeutic applications and developments. Clin Pharmacol Ther. 2008;83(5):761-9.
50. Bose T, Latawiec D, Mondal PP, Mandal S. Overview of nano-drugs characteristics for clinical application: the journey from the entry to the exit point. J Nanopart Res. 2014;16(8):2527.

51. Hoshyar N, Gray S, Han H, Bao G. The effect of nanoparticle size on in vivo pharmacokinetics and cellular interaction. Nanomedicine. 2016;11(6):673-92.
52. Mitragotri S, Burke PA, Langer R. Overcoming the challenges in administering biopharmaceuticals: formulation and delivery strategies. Nat Rev Drug Discovery. 2014;13:655.
53. Bertrand N, Wu J, Xu X, Kamaly N, Farokhzad OC. Cancer nanotechnology: the impact of passive and active targeting in the era of modern cancer biology. Adv Drug Delivery Rev. 2014;66:2-25.
54. Chou LY, Ming K, Chan WC. Strategies for the intracellular delivery of nanoparticles. Chem Soc Rev. 2011;40(1):233-45.
55. Arami H, Khandhar A, Liggitt D, Krishnan KM. In vivo delivery, pharmacokinetics, biodistribution and toxicity of iron oxide nanoparticles. Chem Soc Rev. 2015;44(23):8576-607.
56. Mao Z, Zhou X, Gao C. Influence of structure and properties of colloidal biomaterials on cellular uptake and cell functions. Biomater Sci. 2013;1(9):896-911.
57. Sahay G, Alakhova DY, Kabanov AV. Endocytosis of nanomedicines. J Controlled Release. 2010;145(3):182-95.
58. Pozzi D, Colapicchioni V, Caracciolo G, Piovesana S, Capriotti AL, Palchetti S, et al. Effect of polyethyleneglycol (PEG) chain length on the bio–nano-interactions between PEGylated lipid nanoparticles and biological fluids: from nanostructure to uptake in cancer cells. Nanoscale. 2014;6(5):2782-92.
59. Verhoef JJ, Carpenter JF, Anchordoquy TJ, Schellekens H. Potential induction of anti-PEG antibodies and complement activation toward PEGylated therapeutics. Drug discovery today. 2014;19(12):1945-52.
60. Yang Q, Lai SK. Anti-PEG immunity: emergence, characteristics, and unaddressed questions. Wiley Interdiscip Rev: Nanomed Nanobiotechnol. 2015;7(5):655-77.
61. Bauer M, Lautenschlaeger C, Kempe K, Tauhardt L, Schubert US, Fischer D. Poly (2-ethyl-2-oxazoline) as Alternative for the Stealth Polymer Poly (ethylene glycol): Comparison of in vitro Cytotoxicity and Hemocompatibility. Macromol Biosci. 2012;12(7):986-98.
62. Lila ASA, Nawata K, Shimizu T, Ishida T, Kiwada H. Use of polyglycerol (PG), instead of polyethylene glycol (PEG), prevents induction of the accelerated blood clearance phenomenon against long-circulating liposomes upon repeated administration. Int J Pharm. 2013;456(1):235-42.
63. Wang Y, Zhao Q, Han N, Bai L, Li J, Liu J, et al. Mesoporous silica nanoparticles in drug delivery and biomedical applications. Nanomedicine: (NBM). 2015;11(2):313-27.
64. Janát-Amsbury M, Ray A, Peterson C, Ghandehari H. Geometry and surface characteristics of gold nanoparticles influence their biodistribution and uptake by macrophages. Eur J Pharm Biopharm. 2011;77(3):417-23.
65. Black KC, Wang Y, Luehmann HP, Cai X, Xing W, Pang B, et al. Radioactive 198Au-doped nanostructures with different shapes for in vivo analyses of their biodistribution, tumor uptake, and intratumoral distribution. ACS nano. 2014;8(5):4385-94.

66. Hirn S, Semmler-Behnke M, Schleh C, Wenk A, Lipka J, Schäffler M, et al. Particle size-dependent and surface charge-dependent biodistribution of gold nanoparticles after intravenous administration. Eur J Pharm Biopharm. 2011;77(3):407-16.
67. Champion JA, Mitragotri S. Shape induced inhibition of phagocytosis of polymer particles. Pharmaceutical research. 2009;26(1):244-9.
68. Chen G, Roy I, Yang C, Prasad PN. Nanochemistry and nanomedicine for nanoparticle-based diagnostics and therapy. Chem Rev. 2016;116(5):2826-85.
69. Nazir S, Hussain T, Ayub A, Rashid U, MacRobert AJ. Nanomaterials in combating cancer: therapeutic applications and developments. Nanomedicine: (NBM). 2014;10(1):19-34.
70. Giner-Casares JJ, Henriksen-Lacey M, Coronado-Puchau M, Liz-Marzan LM. Inorganic nanoparticles for biomedicine: where materials scientists meet medical research. Mater Today. 2016;19(1):19-28.
71. Bobo D, Robinson KJ, Islam J, Thurecht KJ, Corrie SR. Nanoparticle-based medicines: a review of FDA-approved materials and clinical trials to date. Pharm Res. 2016;33(10):2373-87.
72. Chen S, Hao X, Liang X, Zhang Q, Zhang C, Zhou G, et al. Inorganic nanomaterials as carriers for drug delivery. J Biomed Nanotechnol. 2016;12(1):1-27.
73. Yang X, Yang MX, Pang B, Vara M, Xia YN. Gold Nanomaterials at Work in Biomedicine. Chem Rev. 2015;115(19):10410-88.
74. Huang XH, Jain PK, El-Sayed IH, El-Sayed MA. Gold nanoparticles: interesting optical properties and recent applications in cancer diagnostic and therapy. Nanomedicine. 2007;2(5):681-93.
75. Li N, Zhao PX, Astruc D. Anisotropic Gold Nanoparticles: Synthesis, Properties, Applications, and Toxicity. Angew Chem, Int Ed. 2014;53(7):1756-89.
76. Huang X, El-Sayed MA. Gold nanoparticles: Optical properties and implementations in cancer diagnosis and photothermal therapy. J Adv Res. 2010;1(1):13-28.
77. Huang XH, Jain PK, El-Sayed IH, El-Sayed MA. Plasmonic photothermal therapy (PPTT) using gold nanoparticles. Lasers Med Sci. 2008;23(3):217-28.
78. Lee SB, Lee HW, Singh TD, Li Y, Kim SK, Cho SJ, et al. Visualization of macrophage recruitment to inflammation lesions using highly sensitive and stable radionuclide-embedded gold nanoparticles as a nuclear bio-imaging platform. Theranostics. 2017;7(4):926.
79. Jing L, Liang X, Deng Z, Feng S, Li X, Huang M, et al. Prussian blue coated gold nanoparticles for simultaneous photoacoustic/CT bimodal imaging and photothermal ablation of cancer. Biomaterials. 2014;35(22):5814-21.
80. Rengan AK, Bukhari AB, Pradhan A, Malhotra R, Banerjee R, Srivastava R, et al. In vivo analysis of biodegradable liposome gold nanoparticles as efficient agents for photothermal therapy of cancer. Nano Lett. 2015;15(2):842-8.
81. Li Z, Huang H, Tang S, Li Y, Yu X-F, Wang H, et al. Small gold nanorods laden macrophages for enhanced tumor coverage in photothermal therapy. Biomaterials. 2016;74:144-54.

82. Cheng X, Sun R, Yin L, Chai Z, Shi H, Gao M. Light-Triggered Assembly of Gold Nanoparticles for Photothermal Therapy and Photoacoustic Imaging of Tumors In Vivo. Adv Mater. 2017;29(6).
83. Sun M, Peng D, Hao H, Hu J, Wang D, Wang K, et al. Thermally Triggered in Situ Assembly of Gold Nanoparticles for Cancer Multimodal Imaging and Photothermal Therapy. ACS Appl Mater Interfaces. 2017;9(12):10453-60.
84. Love JC, Estroff LA, Kriebel JK, Nuzzo RG, Whitesides GM. Self-assembled monolayers of thiolates on metals as a form of nanotechnology. Chem Rev. 2005;105(4):1103-69.
85. Liu JY, Peng QA. Protein-gold nanoparticle interactions and their possible impact on biomedical applications. Acta Biomater. 2017;55:13-27.
86. Deng HH, Wang FF, Shi XQ, Peng HP, Liu AL, Xia XH, et al. Water-soluble gold nanoclusters prepared by protein-ligand interaction as fluorescent probe for real-time assay of pyrophosphatase activity. Biosens Bioelectron. 2016;83:1-8.
87. Gupta A, Moyano DF, Parnsubsakul A, Papadopoulos A, Wang L-S, Landis RF, et al. Ultrastable and biofunctionalizable gold nanoparticles. ACS Appl Mater Interfaces. 2016;8(22):14096–101.
88. Dreaden EC, Alkilany AM, Huang X, Murphy CJ, El-Sayed MA. The golden age: gold nanoparticles for biomedicine. Chem Soc Rev. 2012;41(7):2740-79.
89. Chen Y-S, Frey W, Kim S, Homan K, Kruizinga P, Sokolov K, et al. Enhanced thermal stability of silica-coated gold nanorods for photoacoustic imaging and image-guided therapy. Opt Express. 2010;18(9):8867-78.
90. Jalani G, Cerruti M. Nano graphene oxide-wrapped gold nanostars as ultrasensitive and stable SERS nanoprobes. Nanoscale. 2015;7(22):9990-7.
91. Kreyling WG, Abdelmonem AM, Ali Z, Alves F, Geiser M, Haberl N, et al. In vivo integrity of polymer-coated gold nanoparticles. Nat Nanotechnol. 2015;10(7):619-23.
92. Del Pino P, Yang F, Pelaz B, Zhang Q, Kantner K, Hartmann R, et al. Basic physicochemical properties of polyethylene glycol coated gold nanoparticles that determine their interaction with cells. Angew Chem, Int Ed. 2016;55(18):5483-7.
93. Zhang Z, Liu C, Bai J, Wu C, Xiao Y, Li Y, et al. Silver nanoparticle gated, mesoporous silica coated gold nanorods (AuNR@ MS@ AgNPs): low premature release and multifunctional cancer theranostic platform. ACS Appl Mater Interfaces. 2015;7(11):6211-9.
94. Abadeer NS, Brennan MR, Wilson WL, Murphy CJ. Distance and plasmon wavelength dependent fluorescence of molecules bound to silica-coated gold nanorods. ACS nano. 2014;8(8):8392-406.
95. Li H, Tan L-L, Jia P, Li Q-L, Sun Y-L, Zhang J, et al. Near-infrared light-responsive supramolecular nanovalve based on mesoporous silica-coated gold nanorods. Chem Sci. 2014;5(7):2804-8.
96. Colilla M, Baeza A, Vallet-Regí M. Mesoporous silica nanoparticles for drug delivery and controlled release applications. The Sol-Gel Handbook-Synthesis, Characterization, and Applications: Synthesis, Characterization and Applications, 3-Volume Set. 2015:1309-44.

97. Mamaeva V, Sahlgren C, Lindén M. Mesoporous silica nanoparticles in medicine—recent advances. Adv Drug Delivery Rev. 2013;65(5):689-702.
98. Slowing II, Trewyn BG, Giri S, Lin VY. Mesoporous silica nanoparticles for drug delivery and biosensing applications. Adv Funct Mater. 2007;17(8):1225-36.
99. Lu J, Liong M, Zink JI, Tamanoi F. Mesoporous silica nanoparticles as a delivery system for hydrophobic anticancer drugs. Small. 2007;3(8):1341-6.
100. Kanehara M, Watanabe Y, Teranishi T. Thermally stable silica-coated hydrophobic gold nanoparticles. J Nanosci Nanotechnol. 2009;9(1):673-5.
101. Chen J, Zhang R, Han L, Tu B, Zhao D. One-pot synthesis of thermally stable gold@ mesoporous silica core-shell nanospheres with catalytic activity. Nano Res. 2013;6(12):871-9.
102. Ghosh Chaudhuri R, Paria S. Core/shell nanoparticles: classes, properties, synthesis mechanisms, characterization, and applications. Chem Rev. 2011;112(4):2373-433.
103. Song J-T, Yang X-Q, Zhang X-S, Yan D-M, Wang Z-Y, Zhao Y-D. Facile Synthesis of Gold Nanospheres Modified by Positively Charged Mesoporous Silica, Loaded with Near-Infrared Fluorescent Dye, for in Vivo X-ray Computed Tomography and Fluorescence Dual Mode Imaging. ACS Appl Mater Interfaces. 2015;7(31):17287-97.
104. Liu S, Han M. Synthesis, functionalization, and bioconjugation of monodisperse, Silica-Coated gold nanoparticles: Robust bioprobes. Adv Funct Mater. 2005;15(6):961-7.
105. Kobayashi Y, Correa-Duarte MA, Liz-Marzán LM. Sol− gel processing of silica-coated gold nanoparticles. Langmuir. 2001;17(20):6375-9.
106. Mine E, Yamada A, Kobayashi Y, Konno M, Liz-Marzán LM. Direct coating of gold nanoparticles with silica by a seeded polymerization technique. J Colloid Interface Sci. 2003;264(2):385-90.
107. Caruso F, Spasova M, Salgueiriño-Maceira V, Liz-Marzán L. Multilayer Assemblies of Silica-Encapsulated Gold Nanoparticles on Decomposable Colloid Templates. Adv Mater. 2001;13(14):1090-4.
108. Pastoriza-Santos I, Pérez-Juste J, Liz-Marzán LM. Silica-coating and hydrophobation of CTAB-stabilized gold nanorods. Chem Mater. 2006;18(10):2465-7.
109. Zhao P, Li N, Astruc D. State of the art in gold nanoparticle synthesis. Coord Chem Rev. 2013;257(3):638-65.
110. Nguyen DT, Kim D-J, Kim K-S. Controlled synthesis and biomolecular probe application of gold nanoparticles. Micron. 2011;42(3):207-27.
111. Ahmed S, Ikram S. Biosynthesis of gold nanoparticles: a green approach. J Photochem Photobiol, B. 2016;161:141-53.
112. Murakami T, Tsuchida K. Recent advances in inorganic nanoparticle-based drug delivery systems. Mini-Rev Med Chem. 2008;8(2):175-83.
113. Ferrier Jr RC, Gines G, Gasparutto D, Pépin-Donat B, Rannou P, Composto RJ. Tuning Optical Properties of Functionalized Gold Nanorods through Controlled Interactions with Organic Semiconductors. J Phys Chem C. 2015;119(31):17899-909.

114. Yasun E, Li C, Barut I, Janvier D, Qiu L, Cui C, et al. BSA modification to reduce CTAB induced nonspecificity and cytotoxicity of aptamer-conjugated gold nanorods. Nanoscale. 2015;7(22):10240-8.
115. DuChene JS, Niu W, Abendroth JM, Sun Q, Zhao W, Huo F, et al. Halide anions as shape-directing agents for obtaining high-quality anisotropic gold nanostructures. Chem Mater. 2012;25(8):1392-9.
116. Scarabelli L, Coronado-Puchau M, Giner-Casares JJ, Langer J, Liz-Marzán LM. Monodisperse gold nanotriangles: size control, large-scale self-assembly, and performance in surface-enhanced Raman scattering. ACS nano. 2014;8(6):5833-42.
117. Pelaz B, Grazu V, Ibarra A, Magen C, del Pino P, de la Fuente JM. Tailoring the synthesis and heating ability of gold nanoprisms for bioapplications. Langmuir. 2012;28(24):8965-70.
118. Tian F, Bonnier F, Casey A, Shanahan AE, Byrne HJ. Surface enhanced Raman scattering with gold nanoparticles: effect of particle shape. Anal Methods. 2014;6(22):9116-23.
119. Lohse SE, Murphy CJ. The quest for shape control: a history of gold nanorod synthesis. Chem Mater. 2013;25(8):1250-61.
120. Chandra K, Culver KS, Werner SE, Lee RC, Odom TW. Manipulating the anisotropic structure of gold nanostars using good's buffers. Chem Mater. 2016;28(18):6763-9.
121. Xia X, Xia Y. Gold nanocages as multifunctional materials for nanomedicine. Front Phys. 2014;9(3):378-84.
122. Hua Y, Chandra K, Dam DHM, Wiederrecht GP, Odom TW. Shape-dependent nonlinear optical properties of anisotropic gold nanoparticles. J Phys Chem Lett. 2015;6(24):4904-8.
123. Chen Y-S, Frey W, Kim S, Kruizinga P, Homan K, Emelianov S. Silica-coated gold nanorods as photoacoustic signal nanoamplifiers. Nano Lett. 2011;11(2):348-54.
124. Argyo C, Weiss V, Bräuchle C, Bein T. Multifunctional mesoporous silica nanoparticles as a universal platform for drug delivery. Chem Mater. 2013;26(1):435-51.
125. Sreejith S, Joseph J, Nguyen KT, Murukeshan VM, Lye SW, Zhao Y. Graphene oxide wrapping of gold–silica core–shell nanohybrids for photoacoustic signal generation and bimodal imaging. ChemNanoMat. 2015;1(1):39-45.
126. Hembury M, Chiappini C, Bertazzo S, Kalber TL, Drisko GL, Ogunlade O, et al. Gold-silica quantum rattles for multimodal imaging and therapy. Proc Natl Acad Sci. 2015;112(7):1959-64.
127. Liu J, Detrembleur C, Pauw-Gillet D, Mornet S, Jérôme C, Duguet E. Gold Nanorods Coated with Mesoporous Silica Shell as Drug Delivery System for Remote Near Infrared Light-Activated Release and Potential Phototherapy. Small. 2015;11(19):2323-32.
128. Yang J, Shen D, Zhou L, Li W, Li X, Yao C, et al. Spatially confined fabrication of core-shell gold nanocages@ mesoporous silica for near-infrared controlled photothermal drug release. Chem Mater. 2013;25(15):3030-7.
129. Chen Y, Chen HR, Zeng DP, Tian YB, Chen F, Feng JW, et al. Core/Shell Structured Hollow Mesoporous Nanocapsules: A Potential Platform for Simultaneous Cell Imaging and Anticancer Drug Delivery. ACS nano. 2010;4(10):6001-13.

130. Terentyuk G, Panfilova E, Khanadeev V, Chumakov D, Genina E, Bashkatov A, et al. Gold nanorods with a hematoporphyrin-loaded silica shell for dual-modality photodynamic and photothermal treatment of tumors in vivo. Nano Res. 2014;7(3):325-37.
131. Wang S, Huang P, Nie L, Xing R, Liu D, Wang Z, et al. Single continuous wave laser induced photodynamic/plasmonic photothermal therapy using photosensitizer-functionalized gold nanostars. Adv Mater. 2013;25(22):3055-61.
132. Castillo RR, Colilla M, Vallet-Regi M. Advances in mesoporous silica-based nanocarriers for co-delivery and combination therapy against cancer. Expert Opin Drug Delivery. 2017;14(2):229-43.
133. Li WW, Chen XY. Gold nanoparticles for photoacoustic imaging. Nanomedicine. 2015;10(2):299-320.
134. Cole LE, Ross RD, Tilley JMR, Vargo-Gogola T, Roeder RK. Gold nanoparticles as contrast agents in x-ray imaging and computed tomography. Nanomedicine. 2015;10(2):321-41.
135. Zeng Q, Zhang Y, Ji W, Ye W, Jiang Y, Song J. Inhibitation of cellular toxicity of gold nanoparticles by surface encapsulation of silica shell for hepatocarcinoma cell application. ACS Appl Mater Interfaces. 2014;6(21):19327-35.
136. Thakor AS, Luong R, Paulmurugan R, Lin FI, Kempen P, Zavaleta C, et al. The Fate and Toxicity of Raman-Active Silica-Gold Nanoparticles in Mice. Sci Transl Med. 2011;3(79):79ra33-79ra33.
137. Gao B, Xu J, Shen L, Chen H, Yang H-j, Li A-h, et al. Cellular uptake and intra-organ biodistribution of functionalized silica-coated gold nanorods. Mol Imaging Biol. 2016;18(5):667-76.
138. Lee K-S, El-Sayed MA. Dependence of the enhanced optical scattering efficiency relative to that of absorption for gold metal nanorods on aspect ratio, size, end-cap shape, and medium refractive index. J Phys Chem B. 2005;109(43):20331-8.
139. Hu B, Zhang L-P, Chen X-W, Wang J-H. Gold nanorod-covered kanamycin-loaded hollow SiO 2 (HSKAu rod) nanocapsules for drug delivery and photothermal therapy on bacteria. Nanoscale. 2013;5(1):246-52.
140. Liu W, Zhu Z, Deng K, Li Z, Zhou Y, Qiu H, et al. Gold nanorod@ chiral mesoporous silica core–shell nanoparticles with unique optical properties. J Am Chem Soc. 2013;135(26):9659-64.
141. Chen N-T, Tang K-C, Chung M-F, Cheng S-H, Huang C-M, Chu C-H, et al. Enhanced plasmonic resonance energy transfer in mesoporous silica-encased gold nanorod for two-photon-activated photodynamic therapy. Theranostics. 2014;4(8):798.
142. Monem AS, Elbialy N, Mohamed N. Mesoporous silica coated gold nanorods loaded doxorubicin for combined chemo–photothermal therapy. Int J Pharm. 2014;470(1):1-7.
143. Zhou H, Xu H, Li X, Lv Y, Ma T, Guo S, et al. Dual targeting hyaluronic acid-RGD mesoporous silica coated gold nanorods for chemo-photothermal cancer therapy. Mater Sci Eng, C. 2017;81:261-70.

144. Liu Y, Xu M, Chen Q, Guan G, Hu W, Zhao X, et al. Gold nanorods/mesoporous silica-based nanocomposite as theranostic agents for targeting near-infrared imaging and photothermal therapy induced with laser. Int J Nanomed. 2015;10:4747.
145. Lee C, Hwang HS, Lee S, Kim B, Kim JO, Oh KT, et al. Rabies Virus-Inspired Silica-Coated Gold Nanorods as a Photothermal Therapeutic Platform for Treating Brain Tumors. Adv Mater. 2017;29(13).
146. Hemmer E, Benayas A, Légaré F, Vetrone F. Exploiting the biological windows: current perspectives on fluorescent bioprobes emitting above 1000 nm. Nanoscale Horiz. 2016;1(3):168-84.
147. de Melo-Diogo D, Pais-Silva C, Dias DR, Moreira AF, Correia IJ. Strategies to improve cancer photothermal therapy mediated by nanomaterials. Adv Healthcare Mater. 2017;6(10).
148. Zhang Z, Wang L, Wang J, Jiang X, Li X, Hu Z, et al. Mesoporous silica-coated gold nanorods as a light-mediated multifunctional theranostic platform for cancer treatment. Adv Mater. 2012;24(11):1418-23.
149. Shen S, Tang H, Zhang X, Ren J, Pang Z, Wang D, et al. Targeting mesoporous silica-encapsulated gold nanorods for chemo-photothermal therapy with near-infrared radiation. Biomaterials. 2013;34(12):3150-8.
150. Seo S-H, Kim B-M, Joe A, Han H-W, Chen X, Cheng Z, et al. NIR-light-induced surface-enhanced Raman scattering for detection and photothermal/photodynamic therapy of cancer cells using methylene blue-embedded gold nanorod@ SiO 2 nanocomposites. Biomaterials. 2014;35(10):3309-18.
151. Luo GF, Chen WH, Lei Q, Qiu WX, Liu YX, Cheng YJ, et al. A Triple-Collaborative Strategy for High-Performance Tumor Therapy by Multifunctional Mesoporous Silica-Coated Gold Nanorods. Adv Funct Mater. 2016;26(24):4339-50.
152. Gorelikov I, Matsuura N. Single-step coating of mesoporous silica on cetyltrimethyl ammonium bromide-capped nanoparticles. Nano Lett. 2008;8(1):369-73.
153. Nikoobakht B, El-Sayed MA. Preparation and growth mechanism of gold nanorods (NRs) using seed-mediated growth method. Chem Mater. 2003;15(10):1957-62.
154. Schröder M, Lenting H, Kandelbauer A, Silva CJ, Cavaco-Paulo A, Gübitz GM. Restricting detergent protease action to surface of protein fibres by chemical modification. Appl Microbiol Biotechnol. 2006;72(4):738-44.
155. Shen J, Yin Q, Chen L, Zhang Z, Li Y. Co-delivery of paclitaxel and survivin shRNA by pluronic P85-PEI/TPGS complex nanoparticles to overcome drug resistance in lung cancer. Biomaterials. 2012;33(33):8613-24.
156. Khatibi A, Ma'mani L, Khodarahmi R, Shafiee A, Maghami P, Ahmad F, et al. Enhancement of thermal reversibility and stability of human carbonic anhydrase II by mesoporous nanoparticles. Int J Biol Macromol. 2015;75:67-72.
157. He Q, Zhang J, Shi J, Zhu Z, Zhang L, Bu W, et al. The effect of PEGylation of mesoporous silica nanoparticles on nonspecific binding of serum proteins and cellular responses. Biomaterials. 2010;31(6):1085-92.

158. Yildirim A, Ozgur E, Bayindir M. Impact of mesoporous silica nanoparticle surface functionality on hemolytic activity, thrombogenicity and non-specific protein adsorption. J Mater Chem B. 2013;1(14):1909-20.
159. Gaspar VM, Moreira AF, Costa EC, Queiroz JA, Sousa F, Pichon C, et al. Gas-generating TPGS-PLGA microspheres loaded with nanoparticles (NIMPS) for co-delivery of minicircle DNA and anti-tumoral drugs. Colloids Surf, B. 2015;134:287-94.
160. Pais-Silva C, de Melo-Diogo D, Correia IJ. IR780-loaded TPGS-TOS micelles for breast cancer photodynamic therapy. Eur J Pharm Biopharm. 2017;113:108-17.
161. Yang C, Wu T, Qi Y, Zhang Z. Recent advances in the application of vitamin E TPGS for drug delivery. Theranostics. 2018;8(2):464.
162. Zhang Z, Tan S, Feng S-S. Vitamin E TPGS as a molecular biomaterial for drug delivery. Biomaterials. 2012;33(19):4889-906.
163. Li P-Y, Lai P-S, Hung W-C, Syu W-J. Poly (L-lactide)-vitamin E TPGS nanoparticles enhanced the cytotoxicity of doxorubicin in drug-resistant MCF-7 breast cancer cells. Biomacromolecules. 2010;11(10):2576-82.
164. Jiang G, Park K, Kim J, Kim KS, Oh EJ, Kang H, et al. Hyaluronic acid–polyethyleneimine conjugate for target specific intracellular delivery of siRNA. Biopolymers. 2008;89(7):635-42.
165. Ewe A, Höbel S, Heine C, Merz L, Kallendrusch S, Bechmann I, et al. Optimized polyethylenimine (PEI)-based nanoparticles for siRNA delivery, analyzed in vitro and in an ex vivo tumor tissue slice culture model. Drug Delivery Transl Res. 2017;7(2):206-16.
166. Wu Y, Chu Q, Tan S, Zhuang X, Bao Y, Wu T, et al. D-α-tocopherol polyethylene glycol succinate-based derivative nanoparticles as a novel carrier for paclitaxel delivery. Int J Nanomed. 2015;10:5219.
167. Wang S, Xi W, Cai F, Zhao X, Xu Z, Qian J, et al. Three-photon luminescence of gold nanorods and its applications for high contrast tissue and deep in vivo brain imaging. Theranostics. 2015;5(3):251.
168. Becker J, Trügler A, Jakab A, Hohenester U, Sönnichsen C. The optimal aspect ratio of gold nanorods for plasmonic bio-sensing. Plasmonics. 2010;5(2):161-7.
169. Fröhlich E. The role of surface charge in cellular uptake and cytotoxicity of medical nanoparticles. Int J Nanomed. 2012;7:5577.
170. Jain RK, Stylianopoulos T. Delivering nanomedicine to solid tumors. Nat Rev Clin Oncol. 2010;7(11):653.
171. Kim B-S, Kim C-S, Lee K-M. The intracellular uptake ability of chitosan-coated Poly (D, L-lactideco-glycolide) nanoparticles. Arch Pharmacal Res. 2008;31(8):1050.
172. Roser M, Fischer D, Kissel T. Surface-modified biodegradable albumin nano-and microspheres. II: effect of surface charges on in vitro phagocytosis and biodistribution in rats. Eur J Pharm Biopharm. 1998;46(3):255-63.
173. Kim JM, Chang SM, Kong SM, Kim K-S, Kim J, Kim W-S. Control of hydroxyl group content in silica particle synthesized by the sol-precipitation process. Ceram Int. 2009;35(3):1015-9.

174. Kobler J, Möller K, Bein T. Colloidal suspensions of functionalized mesoporous silica nanoparticles. Acs Nano. 2008;2(4):791-9.
175. Eichler J, Knof J, Lenz H. Measurements on the depth of penetration of light (0.35–1.0 μm) in tissue. Radiat Environ Biophys. 1977;14(3):239-42.
176. Stolik S, Delgado J, Perez A, Anasagasti L. Measurement of the penetration depths of red and near infrared light in human “ex vivo” tissues. J Photochem Photobiol, B. 2000;57(2-3):90-3.
177. Du S, Kendall K, Toloueinia P, Mehrabadi Y, Gupta G, Newton J. Aggregation and adhesion of gold nanoparticles in phosphate buffered saline. J Nanopart Res. 2012;14(3):758.
178. Lequeux M, Grand J, Laurent G. Importance of gold nanorods’ aggregation in surface plasmon coupling with a photochromic film in hybrid structures. Plasmonics. 2015;10(6):1863-8.
179. Huang P, Bao L, Zhang CL, Lin J, Luo T, Yang DP, et al. Folic acid-conjugated Silica-modified gold nanorods for X-ray/CT imaging-guided dual-mode radiation and photo-thermal therapy. Biomaterials. 2011;32(36):9796-809.

Chapter 6

Appendix

6. Appendix

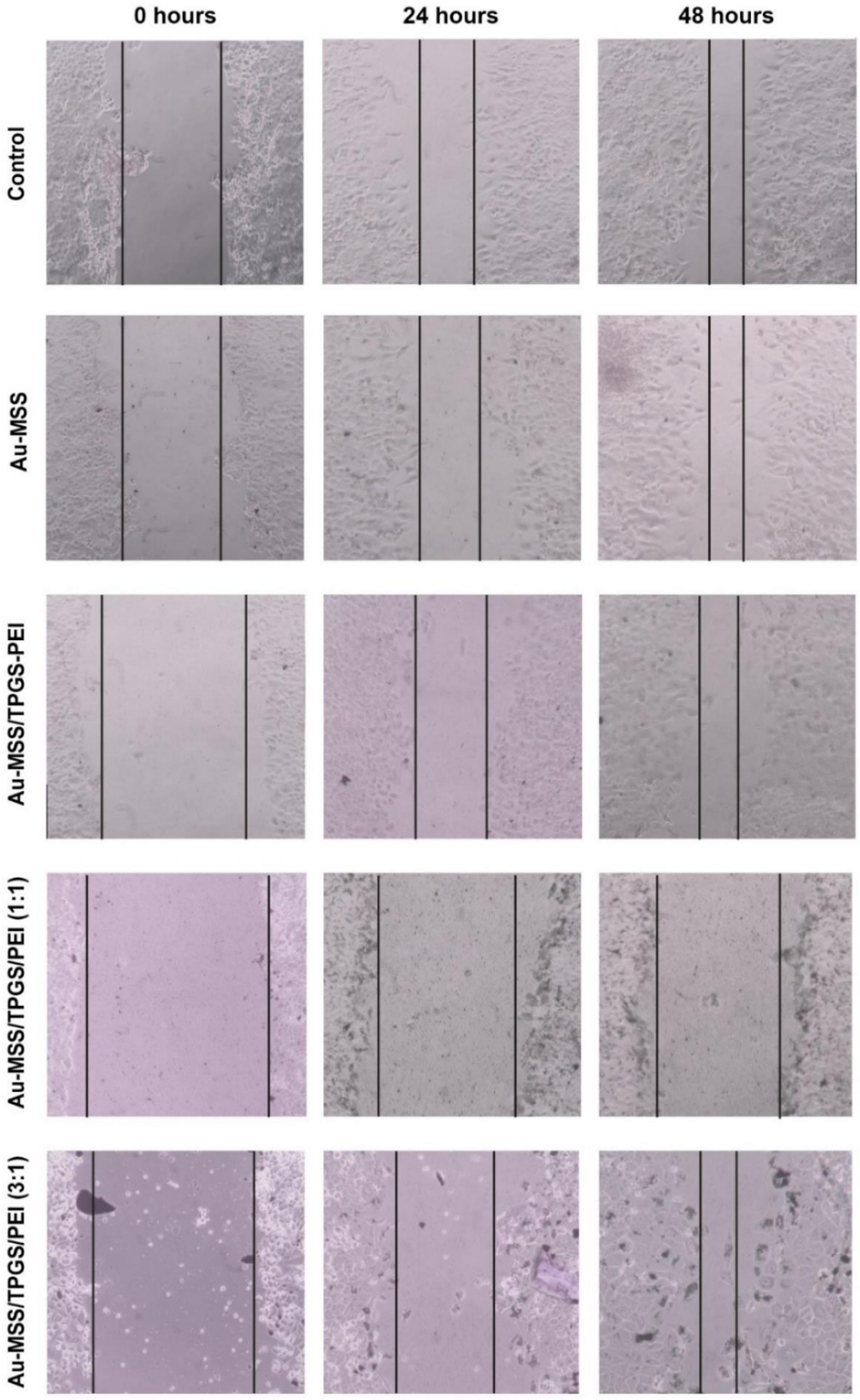

Appendix 1 - Optical microscopy images at 10x magnification of the Au-MSSs effect on the HeLa cells' migration behavior at 0, 24 and 48 h.